Check for updates

A nanovaccine for antigen self-presentation and immunosuppression reversal as a personalized cancer immunotherapy strategy

Chao Liu[1,5], Xue Liu[1,5], Xinchu Xiang[1], Xin Pang[1], Siyuan Chen[1], Yunming Zhang[1], En Ren[1], Lili Zhang[1], Xuan Liu[1], Peng Lv[1], Xiaoyong Wang [1,2], Wenxin Luo[1,2], Ningshao Xia [1,2], Xiaoyuan Chen[3] ✉ and Gang Liu [1,2,4] ✉

The strategy of combining a vaccine with immune checkpoint inhibitors has been widely investigated in cancer management, but the complete response rate for this strategy is still unresolved. We describe a genetically engineered cell membrane nanovesicle that integrates antigen self-presentation and immunosuppression reversal (ASPIRE) for cancer immunotherapy. The ASPIRE nanovaccine is derived from recombinant adenovirus-infected dendritic cells in which specific peptide-major histocompatibility complex class I (pMHC-I), anti-PD1 antibody and B7 co-stimulatory molecules are simultaneously anchored by a programmed process. ASPIRE can markedly improve antigen delivery to lymphoid organs and generate broad-spectrum T-cell responses that eliminate established tumours. This work presents a powerful vaccine formula that can directly activate both native T cells and exhausted T cells, and suggests a general strategy for personalized cancer immunotherapy.

The successful establishment of antitumour immunity requires antigen-specific lymphocytes to undergo activation, expansion and differentiation[1,2]. To a large extent, this process is determined by the interaction between T cells and antigen-presenting cells (APCs). Therefore, the control of APC function is a critical step for therapeutic strategies that require T-cell stimulation. The activation of CD8^{+} cytotoxic T lymphocytes (CTLs) has been proved as a key factor in cancer immunotherapy. This process depends on the tumour-derived peptides that are presented by APCs' major histocompatibility complex class I (MHC-I) molecules to T cells[3-5]. Conventional vaccines, which include peptide and protein vaccines, rely on random encounters with host APCs, and an inappropriate encounter might lead to the silencing of an immune response[6-8]. The activation of CD8^{+} T cells is also excessively dependent on an efficient antigen cross-presentation. Both situations could explain some of the shortcomings of current cancer vaccines.

The high manoeuvrability of the activation programme and cell states is the greatest advantage of adoptive cell therapies, such as chimeric antigen receptor T-cell or dendritic cell (DC) vaccine strategies. Especially for DC-based cancer vaccine strategies, it is possible to induce an endogenous antigen-specific CTL response modulated by a typical MHC-I restricted presentation[9-12]. However, it is unavoidable that the activated DCs are short-lived in the body after injection, and ultimately only a small portion of the administered DCs migrate to the draining lymph nodes (LNs). This disadvantage greatly limits the activation of CTLs[13,14]. Despite the progress made in treating haematological malignancies, the use of chimeric antigen receptor T-cell therapy against solid tumours has not been very

successful[15]. Therefore, it remains a daunting task to design a more effective cancer vaccine formula.

Moreover, in the tumour immune microenvironment, immune checkpoints can inhibit antigen-specific CTL responses[16]. Although immunotherapies based on immune checkpoints have tremendous potential[17-20], only a small fraction of patients experience complete responses, which might be due to the absence of an adequate pre-existing cytotoxic CD8^{+} T-cell response. Stimulating a strong CD8^{+} cell response coupled with immune checkpoint therapy would be an optimal solution. The cellular and molecular mechanisms of checkpoint blockade therapy are yet to be fully elucidated. Some recent studies demonstrated a requirement of CD28 co-stimulation for CD8^{+} T-cell rescue and suggested an important role for the CD28/B7 pathway in PD-1 (programmed cell death protein 1) therapy for cancer patients[21,22]. Therefore, we hypothesized that a co-delivery system with B7-1 and B7-2 co-stimulatory molecules (which are abundant on the surfaces of mature DCs) and an anti-PD-1 antibody may be a key strategy to overcome the challenges faced in cancer immunotherapy.

Biomimetic synthesis involves the synthesis and display of protein cargos on the cell surface, which is a promising strategy for the efficient production of ligand-oriented nanocarriers[23-25]. Such a biosynthesis process could maintain the native conformation, structure and activity of a functional protein of interest[26-28]. In this study, we report a novel nanovaccine formulation that integrates antigen self-presentation and immunosuppression reversal (ASPIRE) for personalized cancer immunotherapy. The ASPIRE nanovaccine is based on artificial cytomembrane nanovesicles (NVs) derived from

531

DCs that feature the directional presentation of specific antigen epitopes by MHC-I molecules, as well as the co-delivery of anti-PD1 antibody and B7 co-stimulatory molecules via a programmed process. It features nanoscale size, good stability and a homing effect that is mediated by surface adhesion molecules. These features enable the ASPIRE nanovaccine to rapidly enrich in the lymphatic system. Unlike conventional vaccines requiring to be delivered to APCs, the ASPIRE nanovaccine has the ability to present neoantigens to CD8+ T cells directly, which we call 'antigen self-presentation', and thus stimulate strong CTL responses. Besides, it also acts as a new enhanced type of checkpoint inhibitor, which strengthens the immunosuppression reversal function of the anti-PD-1 antibody via CD28/B7 co-stimulation and maintains a more sustained CTL response. The ASPIRE nanovaccine shows promise as an efficient strategy to activate strong antitumour immune responses and overcome stubborn immune tolerance.

Engineering and characterization of DC NVs

To induce endogenous presentation, we introduced antigen and stimulated DC differentiation by virus infection. As a proof of principle, we generated a recombinant adenovirus that expresses membrane localization modified green fluorescent protein (rAd-GFP) or ovalbumin (rAd-OVA) (Supplementary Fig. 1a). We also transduced immature DC2.4 cells to express the membrane localization model antigen GFP (Fig. 1a and Supplementary Fig. 1b) and differentiated them into mature DCs (DC-rAd-GFP) (Supplementary Fig. 1c). DCs transduced for 24 hours with rAd-GFP could induce a higher level of MHC-I (Supplementary Fig. 1d,e). This suggests that adenovirus infection promotes the presentation of antigen with MHC-I molecules on DCs. For further verification, we transduced DCs with rAd-OVA, and showed a greater efficacy than those of the other treatments (Supplementary Fig. 2).

DCNV-rAd-Ag was isolated by multistep density gradient ultracentrifugation (Fig. 1b). From 10^8 DCs, 37.43 ± 6.68 mg of DCNVs could be obtained. The NVs had a uniform vesicular morphology (Fig. 1c) and the average diameter was approximately 108 nm (Fig. 1d). In fact, such NVs were found to remain stable for many situations (Supplementary Fig. 3a–c). The content of the main functional membrane proteins on the surface of DCNV-rAd-Ag was similar to that of the parental cells, DC-rAd-Ag (Fig. 1e and Supplementary Fig. 3d)[29,30]. The total proteins of NVs and DCs were then isolated and identified using mass spectrometry. We found that a large number of proteins were upregulated on DCNV-rAd-GFP (Fig. 1f). We found that a variety of co-stimulatory molecules (CD80, CD86, CD40 and so on) were upregulated on DCNV-rAd-GFP. These proteins are known to be involved in the process of antigen presentation and enhance the immune response[31] (Fig. 1g). Notably, we also found the overexpression of various chemokines (CCR2, CCR5, CCR7 and so on) on DCNV-rAd-GFP, which can enhance the migration to LNs[32].

Directly activates naive CD8+ T cells

Based on the characteristics described, we next evaluated the antigen presentation of DCNV-rAd-Ag to naive CD8+ T cells (Fig. 2a). CD8+ T cells from the spleens of C57BL/6 mice were co-cultured with various doses of DCNV-rAd-GFP. The DCNV-rAd-GFP group showed significant T-cell activation in comparison with that of other groups. Consistent results were observed in the activation of primary human T cells (Supplementary Fig. 4). We then examined the impact of DCNV-rAd-Ag on T-cell-specific proliferation. The results showed that the DCNV-rAd-OVA promoted a strong OT-1 CD8+ T-cell proliferation and activation. In contrast, 293TNV-rAd-OVA and blank DCNVs failed to induce a T-cell proliferation or activation (Fig. 2e–g and Supplementary Fig. 5). This suggests that DCNV-rAd-Ags are endowed with the complete surface functional proteins of mature DCs, which can directly present antigens to naive T cells in vitro.

Successfully achieving antigen presentation *in vivo* requires DCNV-rAd-Ags to target LNs and make full contact with T cells. We labelled DCNV-rAd-OVA with indocyanine green (ICG) and quantified the biodistribution after subcutaneous (s.c.) injection at the tail base of mice[24]. The results showed efficient accumulation of DCNV-rAd-OVA in the peripheral LNs within 12 h, whereas the other organs did not reveal a notable fluorescence signal (Fig. 2h,i, Supplementary Fig. 6). The 293TNV-rAd-OVA had a minimal fluorescence signal in the inguinal draining lymph nodes (dLNs). This may be ascribed to the lymphoid homing molecules derived from the mature DC surface, which induced the LN tropism of DCNV-rAd-Ag[29]. C57BL/6 mice were injected subcutaneously at the tail base with DC-rAd-GFP and had a minimal GFP signal in inguinal dLNs after 12 h. In contrast, the DCNV-rAd-GFP group exhibited a markedly increased GFP signal in dLNs (Fig. 2j). Benefiting from its nanoscale size and good stability, DCNV-rAd-Ag can more efficiently overcome tissue barriers and enrich the LNs than whole DCs.

Elicitation of robust CD8+ T-cell responses in vivo

We assessed the systemic T-cell activation of DCNV-rAd-OVA. Splenocytes isolated from animals in the DCNV-rAd-OVA treatment group demonstrated the highest concentration of cytokines after re-stimulation ex vivo with a peptide pool (Fig. 3a). There were enlarged spleens and increased cell numbers in the DCNV-rAd-Ag group, which indicated an efficient stimulation (Supplementary Fig. 7). The control vesicle vaccine 293TNV-rAd-OVA induced only 6–7% Ag-specific CTLs after the third immunization. As a benchmark, we also vaccinated animals with 5 μg of Ag emulsified in aluminium(III) hydroxide (AlumOH), which is the only approved adjuvant in the United States[33,34]. OVA + AlumOH elicited only ~2% Ag-specific CTLs after priming, yet no remarkable T-cell expansion was observed after immunization three times. This is consistent with recent studies regarding a poor performance of recruiting cytotoxic T cells after immunizations with the alum adjuvant[35–37]. In contrast, the DCNV-rAd-OVA group elicited a peak frequency of ~26% Ag-specific CD8+ T cells after the third vaccination (Fig. 3b and Supplementary Figs. 8 and 9). When challenged with 2×10^5 Hep1-6-OVA cells, mice immunized with DCNV-rAd-OVA had no detectable tumour masses. In contrast, mice in other groups succumbed to tumours with only marginal survival benefits (Fig. 3c and Supplementary Fig. 10). We observed different degrees of liver metastasis in the other groups at day 18 after Hep1-6-OVA inoculation, whereas tumour metastasis was effectively prevented in the DCNV-rAd-OVA group (Fig. 3d).

We depleted CD4+ or CD8+ T cells from mice. The results showed that the immunotherapeutic enhancement facilitated by DCNV-rAd-OVA was lost after CD8+ T-cell depletion, but not after CD4+ T-cell depletion (Fig. 3e). The greater therapeutic efficacy also resulted in an improved survival (Supplementary Fig. 11). Thus, it can be concluded that the antitumour effect of DCNV-rAd-Ag is mainly due to the activation of CD8+ T cells. We assessed whether DCNV-rAd-OVA directly present the antigen to CD8+ T cells proactively or deliver the antigen to CD8+ T cells after they are passively taken up by the APCs. This was studied in antigen-presentation-disabled mice in which B7-1/2 on the APCs were knocked out (Fig. 3f and Supplementary Fig. 12). DCNV-rAd-OVA also showed a strong resistance to tumours in B7-1/2$^{-/-}$ mice, but the other groups were unable to inhibit tumour growth in the mice (Fig. 3g). Impressively, the DCNV-rAd-OVA treatment strategy yielded a 100% complete response. Additionally, animals treated with DCNV-rAd-OVA had more peripheral blood CD8+ T cells than those that received other vaccine treatments (Fig. 3h). These data imply that DCNV-rAd-OVA can directly present antigens to CD8+ T cells in vivo and activate a strong and effective antigen-specific CTL response.
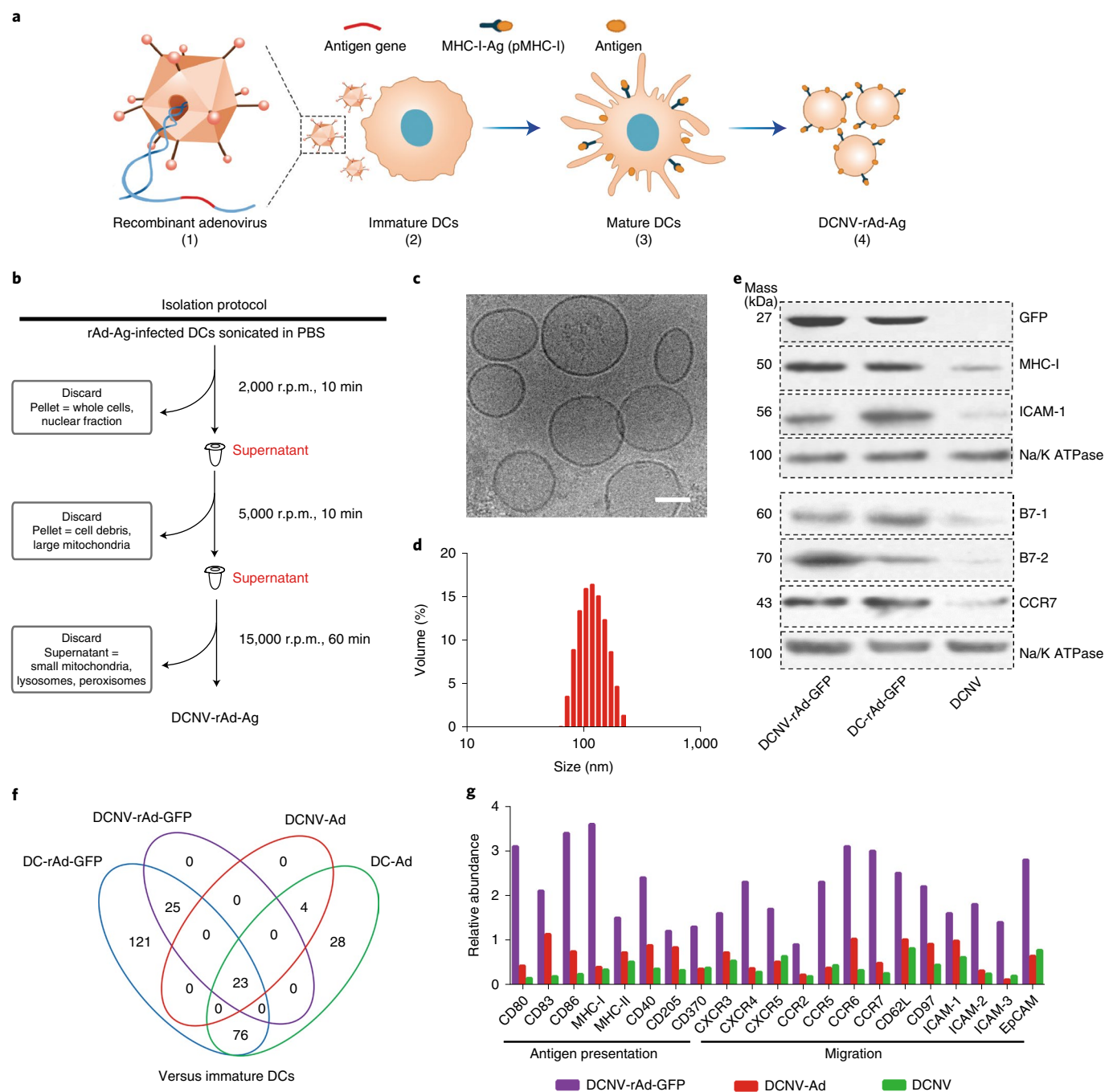
Fig. 1 | Generation and characterization of DCNV-rAd-Ag. a, Generation of DCNVs derived from adenovirus-infected mature dendritic cells. (1) The genes of tumour-specific antigen were genetically engineered into the adenovirus vector. (2) Recombinant adenovirus infected the immature DC2.4 cells to express the modified antigen on the cell surface and stimulate it. (3) Differentiation, maturation and antigen presentation. (4) Harvesting of the induced mature cell membrane and preparation of DCNV-rAd-Ag. **b**, Schematic illustration of the generation of DCNV-rAd-Ag. **c,d**, Cryo-electron microscopy (**c**) and dynamic light scattering analyses (**d**) showed uniform DCNV-rAd-Ag (approximately 108 nm average diameter, polydispersity index = 0.14) with a vesicle-like morphology. Scale bar, 50 nm. **e**, The western blot on membrane proteins from DCNV-rAd-GFP demonstrates a similar protein content on the surface compared to that of the parental cells. Panels **c**–**e** show representative results of two independent experiments with similar results. **f**, Comparison of upregulated immune-response-related proteins in NVs and DCs. **g**, The relative abundance of antigen presentation and migration-related proteins on DCNV-rAd-GFP. r.p.m., revolutions per minute. CCR, CC chemokine receptor; CXCR, C-X-C chemokine receptor; EpCAM, epithelial cellular adhesion molecule; ICAM 1, intercellular adhesion molecule 1; pMHC-I, peptide-major histocompatibility complex class I.

We evaluated the DCNV platform using a B16F10 murine melanoma model to demonstrate its utility for vaccination against neoantigens. This type of tumour is highly aggressive and poorly immunogenic, which thus makes it hard to treat with conventional cancer vaccines[38]. To prevent a tumour immune escape by the loss of a single mutant allele, we sought to elicit broad-spectrum T-cell responses by employing multiple antigens (multiAgs), which included the recently reported B16F10 mutated neoepitopes M27 and M30, as well as tyrosinase-related protein 2 (TRP2), which is a melanoma-associated Ag. These antigens were all engineered on the
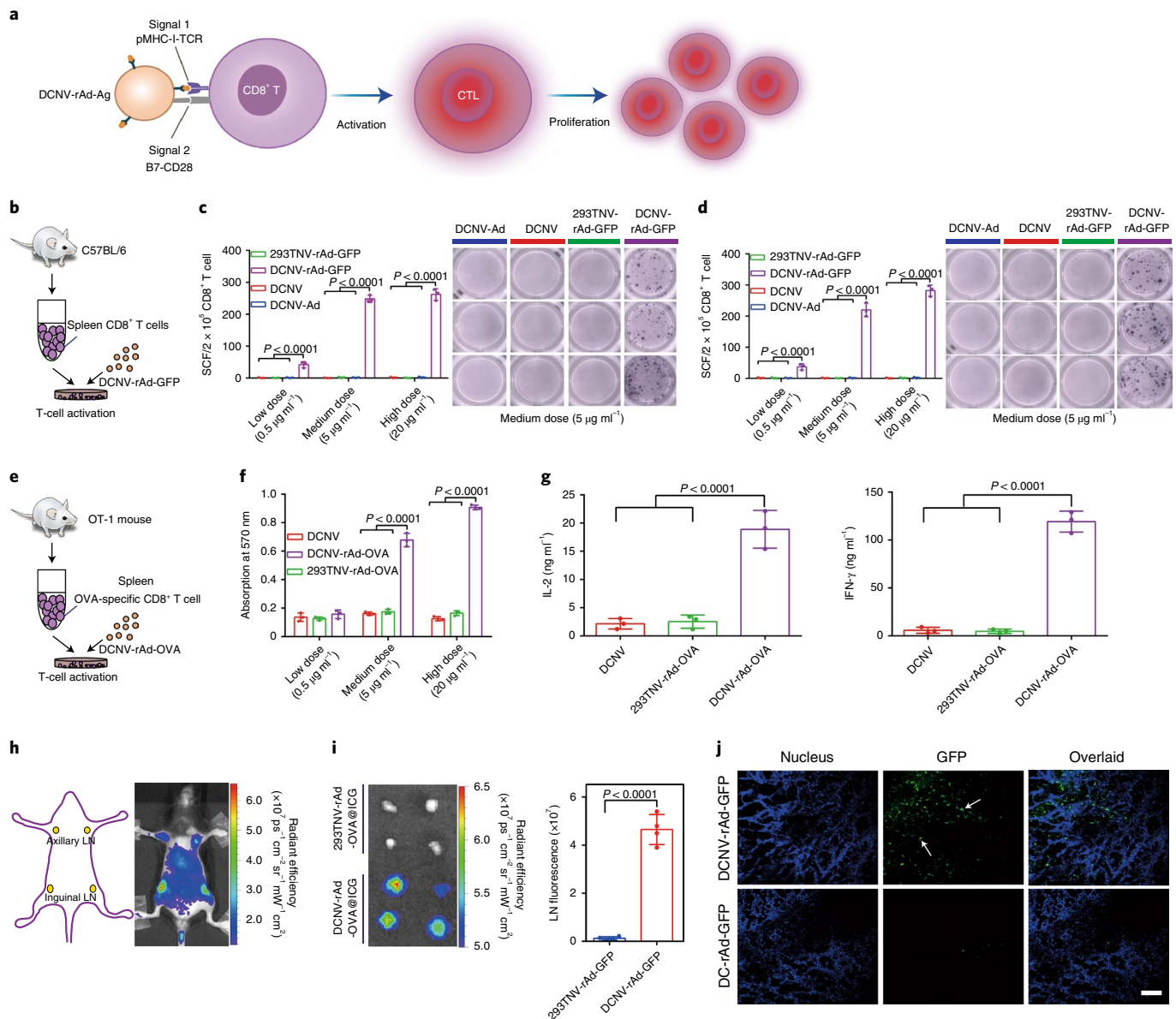
Fig. 2 | DCNV-rAd-Ag for antigen self-presentation and LN targeting. a, Schematic describing DCNV-rAd-Ag for specific activation and proliferation of CD8^{+} T cells. **b–d**, GFP-specific activation of primary mouse T cells: 2×10^5 CD8^{+} T cells, selected from the spleen of C57BL/6 mice, per well were co-cultured with different doses of DCNV-rAd-GFP (0.5, 5 and 20 μg ml^{−1}) (**b**) and enzyme-linked immune absorbent spot (ELISpot) analysis of IFN-γ (**c**) or TNF-α (**d**) spot-forming cells among splenocytes after 7 days of incubation. **e–g**, OVA-specific expansion and activation of primary mouse T cells: 10[5] OT-I CD8^{+} T cells per well were co-cultured with different doses of DCNV-rAd-OVA (0.5, 5 and 20 μg ml[−l]) (**e**), incubation for 24 h, followed by assessment of the T-cell expansion (**f**) and activation (**g**). **h–j**, DCNV-rAd-Ag for LN targeting. C57BL/6 mice were subcutaneously administered at the tail base with 60 μg of ICG-labelled vesicular vaccine or 2×10^5 complete DC vaccine. Fluorescence signals in the draining inguinal LNs of mice treated with ICG-encased DCNV-rAd-OVA (**h**) or 293TNV-rAd-OVA (**i**) were quantified with IVIS after 12 h, or, draining inguinal LNs of mice treated with DCNV-rAd-GFP or DC-rAd-GFP were harvested after 12 h and frozen sections were prepared for confocal microscopy (**j**). Scale bar, 50 μm. The data are shown as the mean ± s.d. from a representative experiment of 2–3 independent experiments with $n = 3$ (**c,d,f,g**) and $n = 4$ (**i**) biologically independent samples. The data were analysed by two-way analysis of variance (ANOVA) (**c,d,f**), one-way ANOVA (**g**) or two-tailed unpaired Student's t-test (**i**) with Bonferroni multiple comparisons post-test. CD8^{+} T, CD8^{+} T cell.

DCNVs. Compared with the traditional multiAgs–AlumOH vaccine, therapeutic vaccination with DCNV-rAd-MultiAgs induced polyfunctional interferon-γ^{+} (IFN-γ^{+}) and IFN-γ^{+} tumour necrosis factor-α^{+} (TNF-α^{+}) multiAgs-specific CD8^{+} T cells and substantially delayed B16F10 tumour growth. However, no tumour rejection was observed in either vaccine group (Supplementary Figs. 13 and 14). This could potentially be due to the immunosuppressive tumour microenvironment, which features high expression levels of

PD-1 and its ligand PD-L1 among dLN CD8^{+} T cells and tumour cells, respectively (Supplementary Fig. 15).

Strong antitumour effect of ASPIRE

ASPIRE was further engineered based on the DCNV platform to break the immunosuppressive PD1/PD-L1 pathway while activating the immune response. The anti-PD1 antibody was pre-expressed on DC surfaces by transmembrane modification[18], and αPD1 DCs
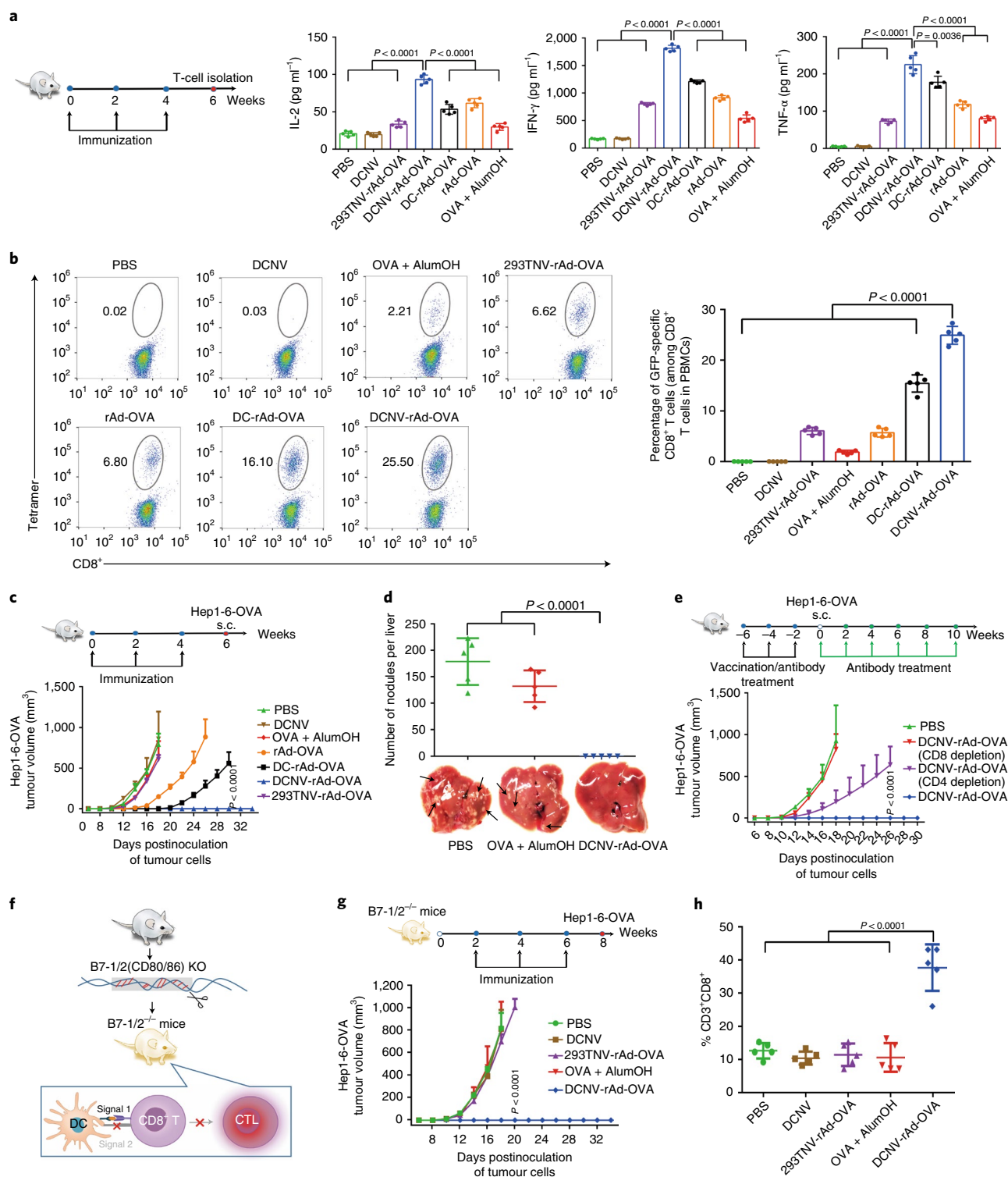
Fig. 3 | DCNV-rAd-Ag for the elicitation of CTL responses. a,b, C57BL/6 mice were immunized with the indicated formulations on days 0, 14 and 28. Enzyme-linked immunosorbent assay (ELISA) analysis of the interleukin 2 (IL-2), TNF-α and IFN-γ production of splenocytes after ex vivo re-stimulation with SIINFEKL on day 42 (**a**), and their representative scatter plots and frequency of SIINFEKL-specific CD8+ T cells in the peripheral blood measured by flow cytometry analysis of tetramer+CD8+ T cells (**b**). **c,d**, Tumour challenge experiments. **c**, On day 42, prevaccinated animals were challenged with a s.c. flank injection of 2×10^5 Hep1-6-OVA cells, and tumour growth was measured over time. **d**, Representative pictures of the lungs and number of liver metastatic nodules counted on day 16 after the Hep1-6-OVA challenge. **e**, Tumour growth (± CD4- or CD8-depleting antibody) in the control or DCNV-rAd-Ag-immunized C57BL/6 mice. **f**, Schematic describing B7-1/2$^{-/-}$ mice. **g,h**, Tumour challenge in antigen-deficient mice. **g**, Vaccinated gene knockout animals were challenged after the final immunization by Hep1-6-OVA cells, and tumour growth was measured over time. **h**, The frequency of peripheral blood CD8+ T cells was measured by flow cytometry analysis. The data are shown as the mean ± s.d. from a representative experiment of 2–3 independent experiments with $n = 5$ (**a–e,g,h**) biologically independent samples. The data were analysed by two-way ANOVA (**c,e,g**) or one-way ANOVA (**a,b,d,h**) with Bonferroni multiple comparisons post-test. CD8+ T, CD8+ T cell.
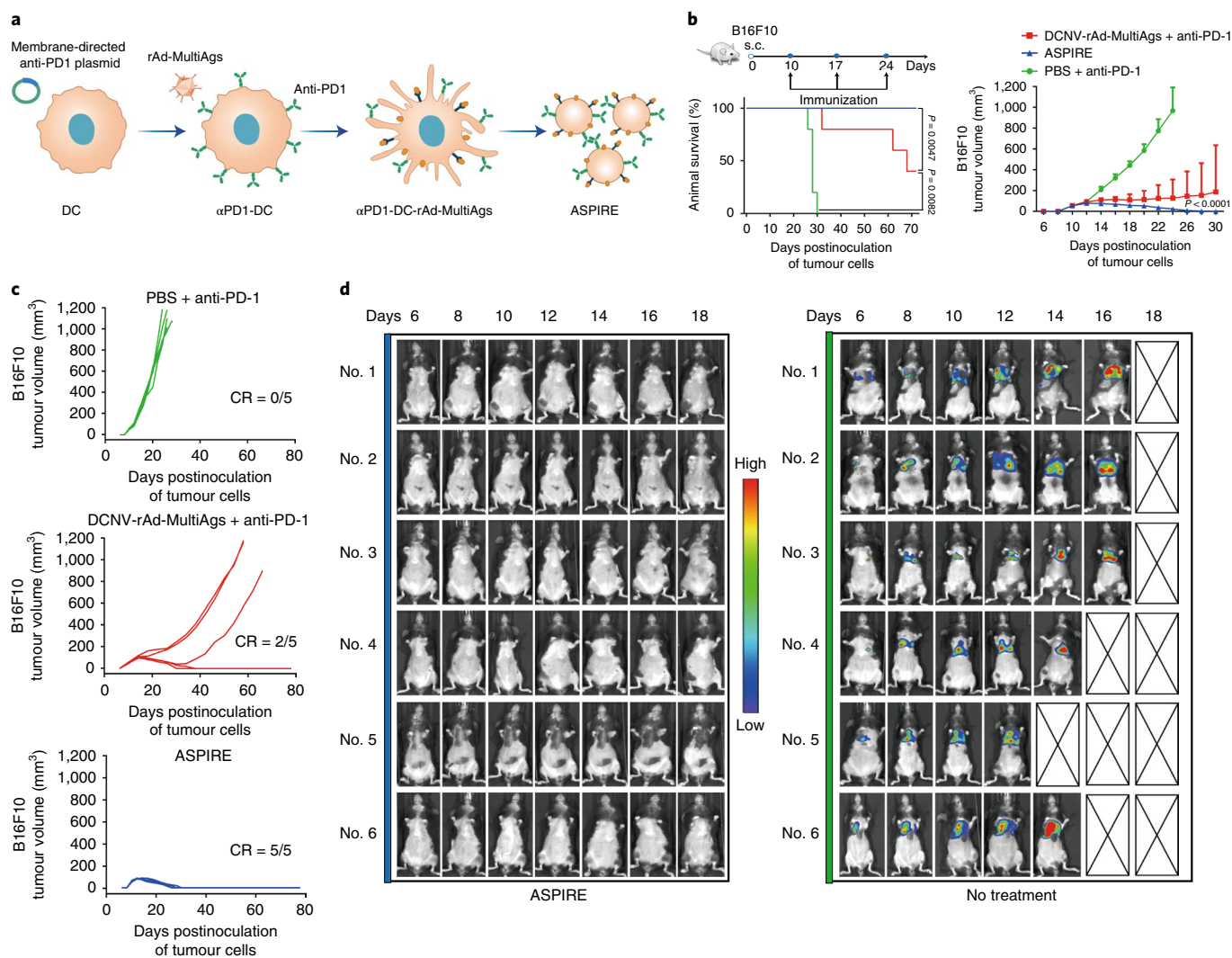
Fig. 4 | ASPIRE vaccine improves the antitumour effect. a, Process for preparing ASPIRE from DCs. **b,c**, C57BL/6 mice were inoculated subcutaneously with 10^5 B16F10 tumour cells and vaccinated with the indicated formulations (60 μg NVs or 10 nmol of each antigen peptide combined with 10.3 μg of anti-PD-1) on days 10, 17 and 24. Average (**b**) and individual (**c**) B16F10 tumour growth curves are shown with the fraction of complete tumour regression (CR). **d**, ASPIRE vaccinated and surviving mice were intravenously rechallenged with 5×10^4 B16-Luc cells two months after the third vaccination. The representative photos show progression of the lung metastases after the B16-Luc challenge. The data are given as the mean ± s.d. from a representative experiment of 2–3 independent experiments with $n = 5$ (**b**) biologically independent samples. The data were analysed by two-way ANOVA (**b**), or log rank (Mantel–Cox) test (**b**) with Bonferroni multiple comparisons post-test.

were obtained. The αPD1 DCs were then induced to translate into αPD1-DC-rAd-MultiAgs by rAd-MultiAgs. After further nanosizing treatment, as mentioned above, ASPIRE was finally prepared (Fig. 4a and Supplementary Fig. 16). ASPIRE treatment led to complete tumour regression in all the mice. In contrast, a tumour regression rate of ~40% occurred when using general combination immunotherapy with DC-rAd-MultiAgs and the same dose of free anti-PD-1 (Fig. 4b,c). Notably, 100% of the surviving mice rejected a subsequent rechallenge with B16F10 cells intravenously injected on day 80 (Fig. 4d). This result indicates that there is a strong immunological memory against tumour recurrence. We speculate that the enhanced antitumour effect may be related to B7-1/2, important co-stimulatory molecules for anti-PD1 therapy[21,22], on the surface of ASPIRE. Importantly, throughout our studies, we did not observe any signs of toxicity, autoimmunity or immune responses directed against the DCNVs in animals that were immunized multiple times with ASPIRE (Supplementary Fig. 17).

B7 co-stimulation enhances anti-PD1-based therapy

We explored whether the co-delivery of B7-1/2 and anti-PD1 promotes immunosuppression reversal and reactivates exhausted CD8+ T cells to restart the CTL response (Fig. 5a). To this end, αPD1-DCNVs were prepared after the αPD1-DCs were induced to maturity by cytokines. We validated the effect using a Lewis lung carcinoma (LLC) model, which is sensitive to anti-PD1 therapy[39,40]. To eliminate interference from T-helper cells, we predepleted CD4+ T cells in mice (Fig. 5b). The results showed that CD8+ T cells isolated from tumours in the αPD1-DCNV treatment group demonstrated the highest percentage of granzyme B (Grz B) and IFN-γ-secreting CD8+ T cells (Fig. 5c). There was rapid tumour growth in all the untreated mice and the mice that received 10 μg of free anti-PD1, whereas αPD1-DCNVs elicited tumour regression in eight of ten animals. In contrast, all the mice that received αPD1-DCNV[B7−/−] (αPD1-DCNVs with B7-1/2 knockout) showed tumour progression.
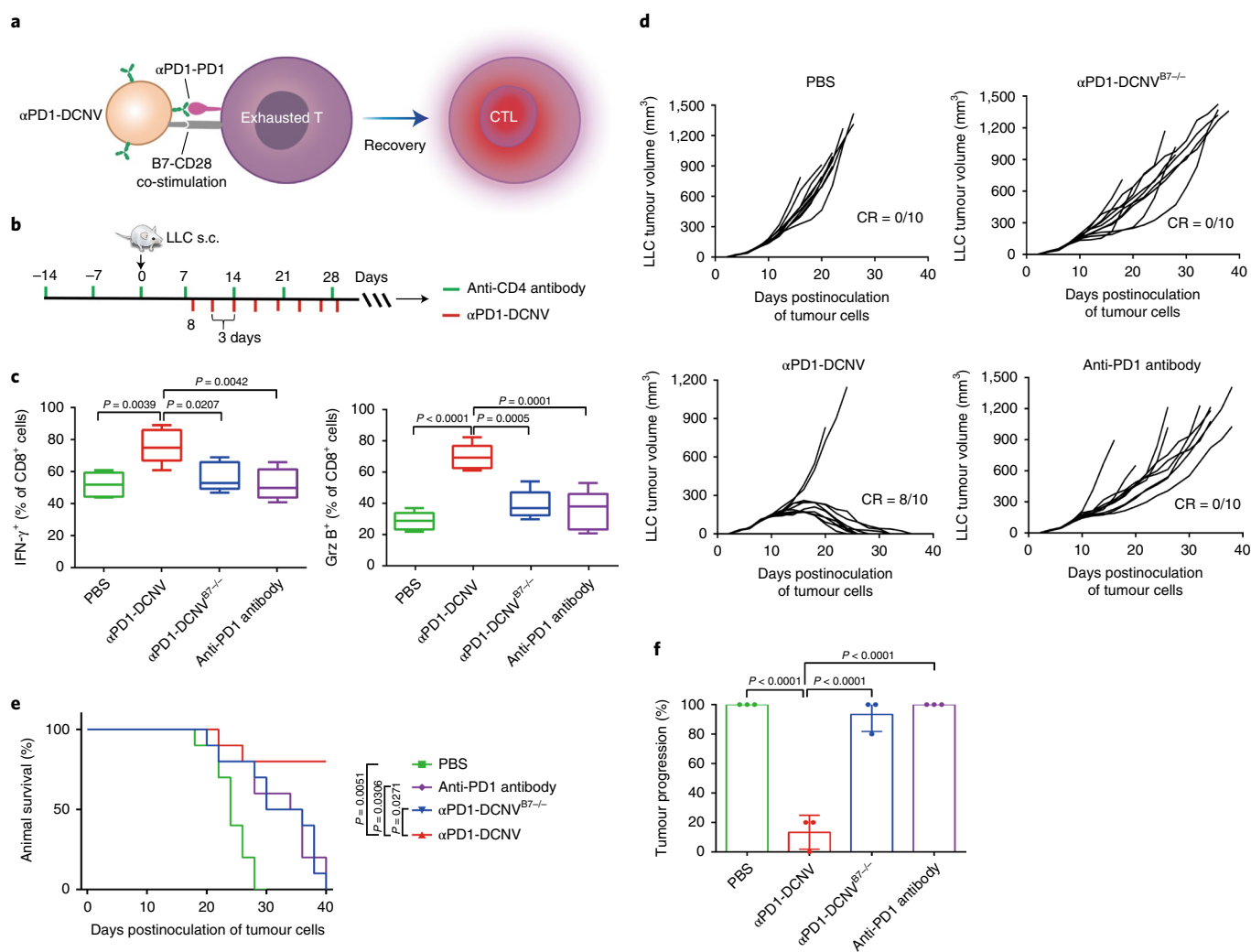
Fig. 5 | B7 co-stimulation enhances the anti-PD1-based immunosuppression reversal. a, Schematic describing ASPIRE for the co-delivery of B7-CD28 and anti-PD1 to promote immunosuppression reversal. **b,** Mice were depleted of CD4+ T cells for the duration of the experiment. LLC tumour-bearing mice were enrolled into different treatment groups as indicated. **c,** The data shown are frequencies of Grz B or IFN-γ that produced tumour-infiltrating CD8+ T cells harvested on day 23 from mice that received different treatment regimens, quantified by flow cytometry analysis with intracellular cytokine staining. **d,** Individual tumour growth, represented by tumour volume. The data show one representative experiment out of three independent experiments. **e,** Survival curves from the data in **d.** The data show one representative experiment (ten mice per group) out of three independent experiments. **f,** Percentage of mice unable to control tumour growth. The data show a summary of three independent experiments with $n=10$ biologically independent samples. For the box plots in **c,** the centre of the box shows the median, the bounds show the interquartile range, the lower whisker extends from the lowest value (minimum) to the 25th percentile and the upper whisker extends from the 76th percentile to the highest value (maximum). The data are shown as the mean ± s.d. from a representative experiment out of three independent experiments with $n=10$ (**c,e**) biologically independent samples. The data were analysed by one-way ANOVA (**c,f**) with Bonferroni multiple comparisons post-test, or log rank (Mantel–Cox) test (**e**). Exhausted T, Exhausted T cell.

The effectiveness of PD1 therapy to suppress LLC tumour growth resulted in a significant improvement in the overall survival of mice treated with αPD1-DCNV in comparison with those of the untreated mice, those treated with free anti-PD1 and those that received αPD1-DCNV[B7−/−]. Furthermore, there was no substantial improvement in the survival of mice treated with αPD1-DCNV[B7−/−] in comparison with those treated with free anti-PD1 (Fig. 5d,e). A summary of three independent experiments is shown in Fig. 5f. As expected, αPD1-DCNV[B7−/−] failed to control the growth of the LLC tumour in mice with a deficiency of B7-1/2 co-stimulatory molecules. Our results show that B7-1/2 co-stimulation is important to enhance anti-PD1 therapy by αPD1-DCNVs.

ASPIRE for immunosuppression reversal

We explored the impact of the ASPIRE integration strategy on the interaction between antigen self-presentation and immunosuppression reversal (Fig. 6a). This was accomplished by using a murine MC-38 colon carcinoma model that harbours an MHC I-restricted neoepitope (ASMTNMELM)[41]. PD-1+CD38hiCD8+ T cells have been described as a population of dysfunctional cells that fail to respond to antigenic stimulation and do not elicit effector functions[42,43]. When ASPIRE (αPD1-DCNV-rAd-neo) was given, there was a significant decrease in the frequency of PD-1+CD38hi in tumour-infiltrating CD8+ T cells and a significant increase in the frequency of tumour-infiltrating antigen-specific CD8+ T cells. Moreover, ~80% of the tumour-infiltrating CD8+ T cells were

IFN-γ[+] and Grz B^{+} T cells. In contrast, 60% IFN-γ[+] and 40% Grz B^{+} T cells were obtained when using the non-integrated combination strategy of ASPIRE groups with αPD1-DCNV+DCNV-rAd-neo (Fig. 6b,c and Supplementary Fig. 18). ASPIRE treatment led to an impressive rate of MC-38 tumour rejection with 100% of the mice being free of tumours. The general combination therapies of αPD1-DCNV+DCNV-rAd-neo and anti-PD1+DCNV-rAd-neo led to tumour regression in ~60% and 20% of the animals, respectively (Fig. 6d).

To understand the reason behind the antitumour effect of ASPIRE, we profiled the T-cell infiltrates in the tumour microenvironment using schedules based on time and sequence difference (Fig. 6e). Vaccination using αPD1-DCNV+DCNV-rAd-neo resulted in a significant decrease in PD-1^{+}CD38^{hi}CD8^{+} T cells in the MC-38 model, which was further decreased when ASPIRE was given. On the other hand, when αPD1-DCNV was given before or after the DCNV-rAd-neo vaccine, the level of total PD-1^{+}CD38^{hi}CD8^{+} T cells was slightly higher or did not change compared to the αPD1-DCNV+DCNV-rAd-neo vaccine group and was significantly higher than that of the ASPIRE group (Fig. 6f). We found that mice treated with ASPIRE had significantly higher levels of central (CD62L^{+}CD44^{+}) and effector (CD62L^{−}CD44^{+}) memory T cells than the other groups (Fig. 6g,h and Supplementary Fig. 19). The concomitant administration of αPD1-DCNV and DCNV-rAd-neo or the administration of αPD1-DCNV three days after the DCNV-rAd-neo vaccination could enhance the memory T cell infiltration. However, administering αPD1-DCNV before the DCNV-rAd-neo vaccine obviously attenuated such an enhancement in the tumour microenvironment. These results are consistent with recent reports that PD-1 blockade in unprimed or suboptimally primed CD8^{+} cells induces resistance through the induction of PD-1^{+}CD38^{hi}CD8^{+} cells[43], and such resistance is reversed by ASPIRE.

Therefore, we consider ASPIRE to be an optimal vaccine strategy for both immune activation and immunosuppression reversal. This bioinspired nanosystem takes advantage of genetically engineered cell membranes as a natural medium for most biological reactions and as an integrated platform to express functional proteins. Specifically, this system shows a promising spatiotemporal effectiveness for multiple co-stimulatory signal transduction.

The remarkable antitumour effect of ASPIRE benefits from various functional protein molecules on its surface, of which the two most important ones are B7-1 and B7-2. The B7-CD28 pathway provides co-stimulatory signals not only for antigen presentation, but also for anti-PD1-based therapy. CTLs were transferred into MC-38 tumour-bearing B7-1/2[−/−] mice and combined with different forms of PD1 therapy (Supplementary Fig. 20), and the results suggest that the B7-CD28 signalling pathway is necessary for

co-stimulation in anti-PD1-based therapy, which is consistent with the latest findings[21,22].

The pressure of tumour vaccine therapy may lead to the selection of target antigen negative cancer cell clones, which is an important mechanism of tumour immune escape. The antitumour efficiency of ASPIRE (αPD1-DCNV-rAd-OVA) was also verified in heterogeneous tumour models with various MC-38 to MC-38-OVA cell ratios, although tumours with 50% or more MC-38 cells escaped immune control (Fig. 6i–m and Supplementary Figs. 21 and 22). Notably, all antigen-presentation-deficient (DC incompetence) mice that received ASPIRE showed tumour progression and the survival of mice with heterogeneous tumours did not substantially improve (Supplementary Fig. 23).

Conclusions

By taking advantage of established manufacturing procedures and excellent safety profiles, the ASPIRE vaccine platform shows notable promise to dramatically improve the delivery of antigens to LNs (Fig. 2). It could also break the general routine of vaccine development, increase the efficiency of antigen presentation through antigen self-presentation and drive CD8^{+} T-cell-dominated immunity against tumours with strong CTL immune responses (Fig. 3). Conventional vaccines often fail to eliminate tumours due to the immunosuppressive PD-L1/PD-1 pathway. ASPIRE integrates antigen self-presentation and immunosuppression reversal, maximizes the cytotoxic potential of T cells, achieves a potently amplified therapeutic effectiveness, effectively suppresses tumour growth and provides long-term immunoprotection (Fig. 4). We also confirmed the important role of the B7-CD28 co-stimulation signal in anti-PD1-based therapy (Fig. 5). B7 co-delivery was applied to anti-PD1-based therapy in a demonstration of antitumour efficacy with a personalized vaccine formula that has the power to directly activate both native T cells and exhausted T cells (Fig. 6).

The present work provides a framework for future clinical translation. The ASPIRE system is designed to induce neoantigen-specific CTL immunity, which requires the identification and screening of tumour neoantigens. This can be achieved with the rapid development of sequencing technology. The recent biomedical breakthroughs in whole-exome sequencing, immunogenomics and computational immunology provided technologies for the comprehensive exploitation of neoantigens for clinical applications[44–47]. It is also worth mentioning that, although the production of the ASPIRE formulation is somewhat more complicated than that of a DC vaccine, the chemistry, manufacturing and control of ASPIRE are not a major concern as we have established a standard operating procedure for a scaled synthesis with a proper quality control of the membrane vesicles. Compared with conventional DC vaccines,

Fig. 6 | ASPIRE vaccine enhances immunotherapy by integrating antigen self-presentation and immunosuppression reversal, and induces cascade immune responses in heterogeneous tumours. a, Schematic describing ASPIRE for antigen self-presentation and immunosuppression blockade. **b**, C57BL/6 mice were inoculated subcutaneously with 3×10^5 MC-38 tumour cells and vaccinated with the indicated formulations (60 μg of NVs or combined with 100 μl of anti-PD1 antibody) on days 10, 17 and 24. **c**, The frequency of CD38^{hi} or antigen-specific T cells in tumour-infiltrating CD8^{+} T cells, and percentages of Grz B or IFN-γ that produced tumour-infiltrating CD8^{+} T cells harvested on day 20 from mice that received different treatment regimens quantified by flow cytometry analysis with intracellular cytokine staining. **d**, Individual MC-38 tumour growth curves with the fraction of complete tumour regression and survival monitored over time. **e**, Schedule of mouse treatments. Tumour-infiltrating T cells were collected 7 days after treatment. **f**, Frequency of PD-1^{+}CD38^{hi} cells in the total CD8^{+} T cells. **g**, Schedule of mouse treatments. Tumour-infiltrating central and effector memory T cells were collected 17 days after treatment. **h**, Frequency of CD62L^{+}CD44^{+} and CD62L^{−}CD44^{+} cells in the total CD8^{+} T cells after various treatments. **i**, C57BL/6 mice were inoculated subcutaneously with 3×10^5 heterogeneous tumour cells (2.4×10^5 MC-38-OVA cells mixed with 6×10^4 MC-38 cells) and vaccinated with the indicated formulations (60 μg of NVs, 2×10^5 DCs or 0.2 nmol OVA) on days 10, 17 and 24. **j**, The proportions of OVA-negative tumour cells in the tumour tissue of the phosphate buffered solution (PBS) group detected on days 10 and 20. **k**, Shown are the percentages of mature DCs (CD11c^{+}CD80^{+}MHCII^{+}) in tumour-infiltrating DCs on day 20. **l**, Survival curves. **m**, Individual tumour growth curves are shown with the fraction of complete tumour regression (CR). For box plots in **c**, **f** and **h**, the centre of the box shows the median, the bounds show the interquartile range, the lower whisker extends from the lowest value (minimum) to the 25th percentile and the upper whisker extends from the 76th percentile to the highest value (maximum). The data are shown as the mean ± s.d. from a representative experiment of 2–3 independent experiments with $n = 10$ biologically independent samples. The data were analysed by one-way ANOVA (**c,k**) with Bonferroni multiple comparisons post-test, or log rank (Mantel–Cox) test (**d,l**). NS, not significant.
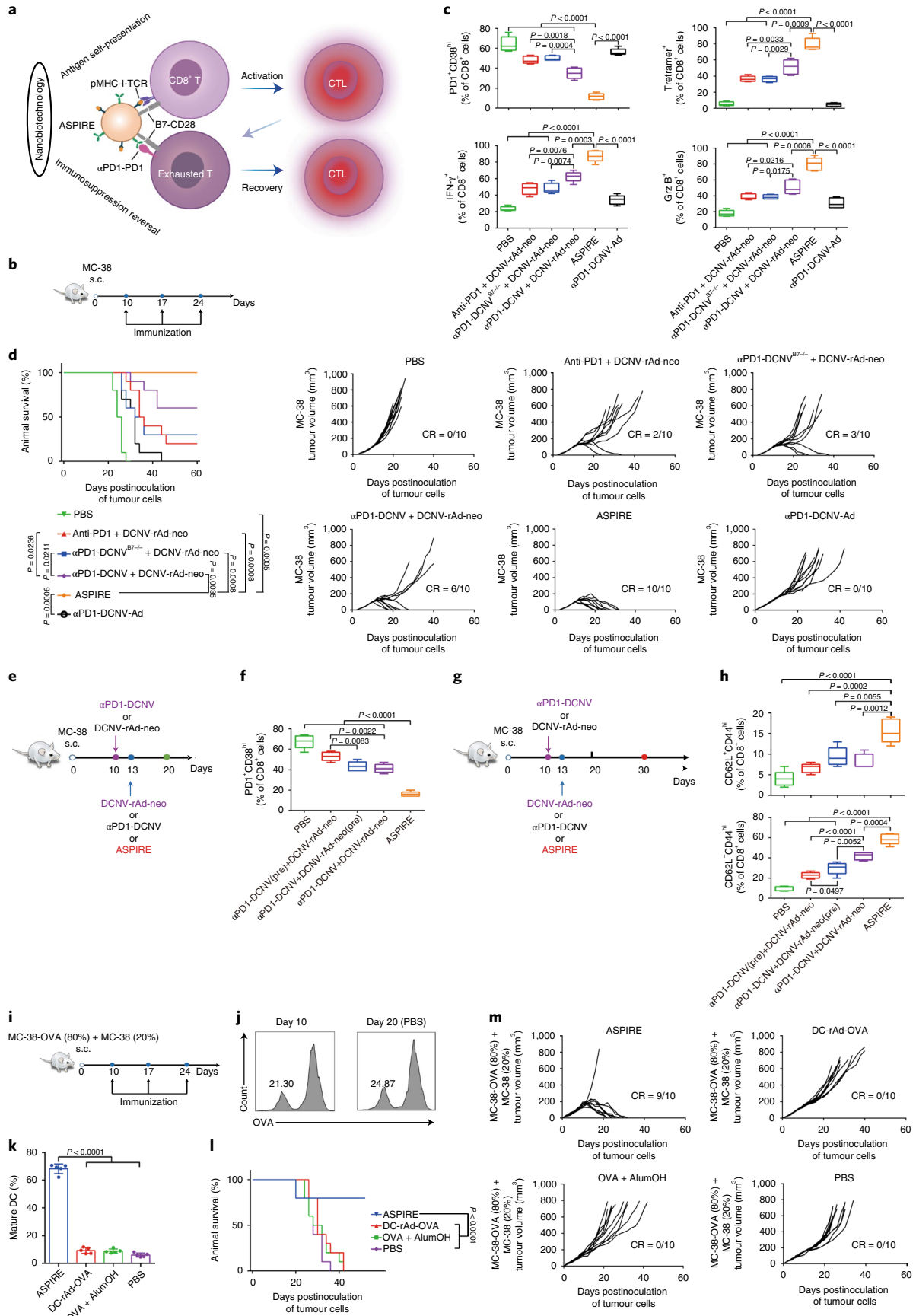
cell-free ASPIRE has unique advantages in storage and long-distance transportation, which greatly reduces the production cost and labour intensiveness (Supplementary Fig. 24).

In conclusion, we have developed a novel nanovaccine platform with the ability to activate the immune response and break immune tolerance. We have demonstrated its ability to stimulate powerful CTL responses and enhance the immune checkpoint blockade with a remarkable therapeutic efficacy. Owing to the tolerance of ASPIRE to a large protein insertion in a natural form, our approach provides a powerful and facile way to produce personalized cancer vaccines. Furthermore, this platform technology may be generally applicable to treat other diseases as well, such as chronic viral infection, in which T-cell exhaustion often occurs during infection and prevents the optimal viral control[48,49].

Online content

References

1. Couzin-Frankel, J. Cancer immunotherapy. *Science* **342**, 1432–1433 (2013).
2. Chen, D. S. & Mellman, I. Oncology meets immunology: the cancer-immunity cycle. *Immunity* **39**, 1–10 (2013).
3. Huppa, J. B. & Davis, M. M. T-cell-antigen recognition and the immunological synapse. *Nat. Rev. Immunol.* **3**, 973–983 (2003).
4. Fuertes, M. B. et al. Host type I IFN signals are required for antitumor CD8+ T cell responses through CD8α+ dendritic cells. *J. Exp. Med.* **208**, 2005–2016 (2011).
5. Steinman, R. M. Decisions about dendritic cells: past, present, and future. *Annu. Rev. Immunol.* **30**, 1–22 (2012).
6. Heath, W. R. & Carbone, F. R. Cross-presentation, dendritic cells, tolerance and immunity. *Annu. Rev. Immunol.* **19**, 47–64 (2001).
7. Heath, W. R. & Carbone, F. R. Cross-presentation in viral immunity and self-tolerance. *Nat. Rev. Immunol.* **1**, 126–134 (2001).
8. Albert, M. L. & Bhardwaj, N. Resurrecting the dead: DCs cross-present antigen derived from apoptotic cells on MHC I. *Immunologist* **6**, 194–198 (1998).
9. Palucka, A. K. et al. Dendritic cells loaded with killed allogeneic melanoma cells can induce objective clinical responses and MART-1 specific CD8+ T-cell immunity. *J. Immunother.* **29**, 545–557 (2006).
10. Steinman, R. M. & Bancherau, J. Taking dendritic cells into medicine. *Nature* **449**, 419–426 (2007).
11. Palucka, K. & Banchereau, J. Cancer immunotherapy via dendritic cells. *Nat. Rev. Cancer* **12**, 265–277 (2012).
12. Bancherau, J. & Steinman, R. M. Dendritic cells and the control of immunity. *Nature* **392**, 245–252 (1998).
13. Nopora, A. & Brocker, T. Bcl-2 controls dendritic cell longevity in vivo. *J. Immunol.* **169**, 3006–3014 (2002).
14. Park, D., Lapteva, N., Seethammagari, M., Slawin, K. M. & Spencer, D. M. An essential role for Akt1 in dendritic cell function and tumor immunotherapy. *Nat. Biotechnol.* **24**, 1581–1590 (2006).
15. Shah, N. N. & Fry, T. J. Mechanisms of resistance to CAR T cell therapy. *Nat. Rev. Clin. Oncol.* **16**, 372–385 (2019).
16. Ribas, A. & Wolchok, J. D. Cancer immunotherapy using checkpoint blockade. *Science* **359**, 1350–1355 (2018).
17. Garon, E. B. et al. Pembrolizumab for the treatment of non-small-cell lung cancer. *N. Engl. J. Med.* **372**, 2018–2028 (2015).
18. Wolchok, J. D. et al. Nivolumab plus ipilimumab in advanced melanoma. *N. Engl. J. Med.* **369**, 122–133 (2013).
19. Hamid, O. et al. Safety and tumor responses with lambrolizumab (anti-PD-1) in melanoma. *N. Engl. J. Med.* **369**, 134–144 (2013).
20. Brahmer, J. R. et al. Safety and activity of anti-PD-L1 antibody in patients with advanced cancer. *N. Engl. J. Med.* **366**, 2455–2465 (2012).
21. Hui, E. F. et al. T cell costimulatory receptor CD28 is a primary target for PD-1-mediated inhibition. *Science* **355**, 1428–1433 (2017).
22. Kamphorst, A. O. et al. Rescue of exhausted CD8 T cells by PD-1-targeted therapies is CD28-dependent. *Science* **355**, 1423–1427 (2017).
23. Chen, Z. W., Wang, Z. J. & Gu, Z. Bioinspired and biomimetic nanomedicines. *Acc. Chem. Res.* **52**, 1255–1264 (2019).
24. Zhang, P. F. et al. Genetically engineered liposome-like nanovesicles as active targeted transport platform. *Adv. Mater.* **30**, 1705350 (2018).
25. Hu, C. M. J. et al. Nanoparticle biointerfacing by platelet membrane cloaking. *Nature* **526**, 118–121 (2015).
26. Liu, X. et al. Vesicular antibodies: a bioactive multifunctional combination platform for targeted therapeutic delivery and cancer immunotherapy. *Adv. Mater.* **31**, 1808294 (2019).
27. Zhang, P. F. et al. Virus-mimetic nanovesicles as a versatile antigen-delivery system. *Proc. Natl Acad. Sci. USA* **112**, E6129–E6138 (2015).
28. Liu, X. et al. Bioinspired artificial nanodecoys for hepatitis B virus. *Angew. Chem. Int. Ed.* **57**, 12499–12503 (2018).
29. Sallusto, F., Lenig, D., Forster, R., Lipp, M. & Lanzavecchia, A. Two subsets of memory T lymphocytes with distinct homing potentials and effector functions. *Nature* **401**, 708–712 (1999).
30. Munro, J. M. Endothelial-leukocyte adhesive interactions in inflammatory diseases. *Eur. Heart J.* **14**, 72–77 (1993).
31. Chen, L. & Flies, D. B. Molecular mechanisms of T cell co-stimulation and co-inhibition. *Nat. Rev. Immunol.* **13**, 227–242 (2013).
32. Worbs, T., Hammerschmidt, S. I. & Forster, R. Dendritic cell migration in health and disease. *Nat. Rev. Immunol.* **17**, 30–48 (2017).
33. Li, H. Y., Li, Y. H., Jiao, J. & Hu, H. M. Alpha-alumina nanoparticles induce efficient autophagy-dependent cross-presentation and potent antitumour response. *Nat. Nanotechnol.* **6**, 645–650 (2011).
34. Flach, T. L. et al. Alum interaction with dendritic cell membrane lipids is essential for its adjuvanticity. *Nat. Med.* **17**, 479–487 (2011).
35. Wheeler, C. M. et al. Efficacy, safety, and immunogenicity of the human papillomavirus 16/18 AS04-adjuvanted vaccine in women older than 25 years: 7-year follow-up of the phase 3, double-blind, randomised controlled VIVIANE study. *Lancet Infect. Dis.* **16**, 1154–1168 (2016).
36. Zhu, F. C. et al. Efficacy and safety of a recombinant hepatitis E vaccine in healthy adults: a large-scale, randomised, double-blind placebo-controlled, phase 3 trial. *Lancet* **376**, 895–902 (2010).
37. Leslie, M. Solution to vaccine mystery starts to crystallize. *Science* **341**, 26–27 (2013).
38. Verdegaal, E. M. E. et al. Neoantigen landscape dynamics during human melanoma–T cell interactions. *Nature* **536**, 91–95 (2016).
39. Bertrand, F. et al. TNF alpha blockade overcomes resistance to anti-PD-1 in experimental melanoma. *Nat. Commun.* **8**, 2256 (2017).
40. Li, H. Y. et al. The tumor microenvironment regulates sensitivity of murine lung tumors to PD-1/PD-L1 antibody blockade. *Cancer Immunol. Res.* **5**, 767–777 (2017).
41. Yadav, M. et al. Predicting immunogenic tumour mutations by combining mass spectrometry and exome sequencing. *Nature* **515**, 572–576 (2014).
42. Chen, L. M. et al. CD38-mediated immunosuppression as a mechanism of tumor cell escape from PD-1/PD-L1 blockade. *Cancer Discov.* **8**, 1156–1175 (2018).
43. Verma, V. et al. PD-1 blockade in subprimed CD8 cells induces dysfunctional PD-1+CD38hi cells and anti-PD-1 resistance. *Nat. Immunol.* **20**, 1555–1555 (2019).
44. Bulik-Sullivan, B. et al. Deep learning using tumor HLA peptide mass spectrometry datasets improves neoantigen identification. *Nat. Biotechnol.* **37**, 55–63 (2019).
45. Robbins, P. F. et al. Mining exomic sequencing data to identify mutated antigens recognized by adoptively transferred tumor-reactive T cells. *Nat. Med.* **19**, 747–752 (2013).
46. Liu, X. S. & Mardis, E. R. Applications of immunogenomics to cancer. *Cell* **168**, 600–612 (2017).
47. Schumacher, T. N. & Schreiber, R. D. Neoantigens in cancer immunotherapy. *Science* **348**, 69–74 (2015).
48. Im, S. J. et al. Defining CD8+ T cells that provide the proliferative burst after PD-1 therapy. *Nature* **537**, 417–421 (2016).
49. Blackburn, S. D. et al. Coregulation of CD8+ T cell exhaustion by multiple inhibitory receptors during chronic viral infection. *Nat. Immunol.* **10**, 29–37 (2009).

Methods

Mice and cell lines. All the animals were cared for and treated according to the instructions and approval of the Institutional Animal Care and Use Committee of Xiamen University. Male and female C57Bl/6 mice (6–8 weeks old) were purchased from SLAC (Shanghai). B7-1/2-deficient mice with a C57BL/6 genetic background were generated by the Xiamen University Laboratory Animal Center. OT-1 mice were provided by the Chinese Academy of Medical Sciences. The mice were maintained under specific pathogen-free conditions in the animal facility at Xiamen University. 293T HEK, DC2.4, Hep1-6-OVA, B16F10, B16F10-Luc, MC-38, MC-38-OVA and LLC cells were acquired from the National Institute of Diagnostics and Vaccine Development in Infectious Diseases (Xiamen University). For the isolation of T cells from spleen or tumour tissue, the Pan T-cell Isolation Kit (Miltenyi Biotec) was used. For the isolation of CD8+ T cells, peripheral blood monocytes (PBMCs) from volunteers were isolated, or spleens from C57BL/6 or OT-1 mice were digested by Liberase (Roche Diagnostics) and DNase I (SIGMA-ALDRICH) to generate single-cell suspensions, which were then stained with R-phycoerythrin (PE)-conjugated anti-CD8 antibody and applied to anti-PE microbeads (Miltenyi Biotec) for isolation. Human PBMCs were freshly isolated from Chinese healthy adult volunteers with informed consent. All the experiments that used human PBMCs were approved by the Medical Ethics Committee of the School of Public Health of Xiamen University. Splenic lymphocytes were isolated by a splenic lymphocyte kit (Dakewe Biotech). Unless otherwise specified, DC2.4 is referred to as DC in the article. DC2.4 cells were cultured in a medium with rmGM-CSF (recombinant granulocyte-macrophage colony-stimulating factor)and rmIL-4 (all purchased from ThermoFisher). The culture medium used for DCs and T cells was RPMI-1640 (Gibco), supplemented with 10% fetal bovine serum, 100 U ml⁻¹ penicillin (Invitrogen) and 100 μg ml⁻¹ streptomycin (Invitrogen). The culture medium used for 293T HEK, Hep1-6-OVA, B16F10, B16F10-Luc, MC-38, MC-38-OVA and LLC cells was Dulbecco′s Modified Eagle Medium (Gibco) supplemented with 10% fetal bovine serum, 100 U ml⁻¹ penicillin and 100 μg ml⁻¹ streptomycin. Throughout the studies, all the cells were used as received and tested negative for mycoplasma contamination and rodent pathogens.

Recombinant adenovirus construction. A signal sequence led by a Kozak consensus sequence was fused in a frame to the N terminus of an antigen protein/epitope (GFP/OVA, or M27-M30-TRP2/ASMTNMELM with ten copies) gene-constant region, a PDGFR transmembrane domain was fused to the C terminus and a FLAG Tag fused after the transmembrane domain to analyse the epitope expression[26,27]. The frame was cloned to shuttle plasmid vector pDC316. Finally, the recombinant adenovirus (rAd-GFP/OVA, rAd-MultiAgs and rAd-neo) was produced using the simple system of AdMax (Ad5) (Supplementary Fig. 1). The sequences were designed and analysed with Snapgene (version 2.3.2).

Preparation of DC-rAd-Ag. Immature DC2.4 cells were plated at 1×10^6 cells per well in 12-well plates. After 24 h, the DCs were infected with a recombinant adenovirus titre of 100 multiplicity of infection (MOI), or cells in the control groups were incubated with 20 μg of pDC316-GFP or 50 μg of antigen proteins in various formulations (that is, PBS/Ag/Liposome@Ag/Ag@IONPs), in complete media with the addition of a maturation factor combination (1,000 U ml⁻¹ rmGM-CSF, 1,000 U ml⁻¹ rmIL-4 and 200 U ml⁻¹ rmTNF-α) for different lengths of time (2, 6, 24 and 48 h) at 37 °C with 5% CO₂. DCs were harvested, washed with FACS buffer (1% fetal bovine serum in PBS), incubated with anti-CD16/32 (Biolegend) at room temperature and then stained on ice with anti-B7-1-APC/anti-B7-2-FITC/anti-MHC-I(H-2Kᵇ)-PE antibodies or PE-conjugated antimouse SIINFEKL/H-2Kᵇ monoclonal antibody 25-D1.16 (all purchased from eBioscience). Cells were analysed by flow cytometry (Cyan 5, Beckman Coulter). DCs cultured in medium with 1,000 U ml⁻¹ rmGM-CSF and 1,000 U ml⁻¹ rmIL-4 were stained as the background to quantify the MHC-I expression level.

Preparation and characterization of DCNV-rAd-Ag. Immature DC2.4 cells were infected with a recombinant adenovirus titre of 100 MOI, and cultured in the medium with the addition of a maturation factor combination for 24 h.

According to our previous work[26–28], the cells were collected and washed in cold PBS mixed with protease inhibitor twice to remove cellular debris and culture medium. Next, the cells were suspended in saline and sonicated in a sterile 1.5 ml EP tube under a low power (22.5 W, 1 min) on ice. Then the NVs were isolated by multistep density gradient ultracentrifugation before being resuspended in saline. The product was then introduced to a Mini-Extruder (Avanti Polar Lipids) equilibrated in saline (200 nm pore-sized membrane filters) to further purify uniform NVs (DCNV-rAd-Ag).

DCNV-rAd-MultiAgs wash, DCNV-Ad was prepared from DC2.4 cells that had been infected with a blank adenovirus titre of 100 MOI for 24 h, DCNV was prepared from DC2.4 cells without any treatment, 293TNV-rAd-Ag was prepared from 293T HEK cells that had been infected with a rAd-Ag titre of 100 MOI for 24 h. All the NVs were prepared as mentioned above.

hDCNV-rAd-Ag/hDCNV-Ad/hDCNV was prepared from DCs of human PBMCs. Briefly, human PBMCs were isolated from healthy blood donors using Ficoll density gradient centrifugation (Biocoll, Biochrom AG). CD14-positive monocytes were isolated by MACS selection (Miltenyi), and cultured for 5 days in complete media with the addition of a stimulating factor combination (1,000 U ml⁻¹ rhGM-CSF and 1,000 U ml⁻¹ rhIL-4), and then immature DCs were obtained. Immature DCs were infected with a recombinant adenovirus titre of 100 MOI, and cultured in the medium with the addition of a maturation factor combination (1,000 U ml⁻¹ rhGM-CSF, 1000 U ml⁻¹ rhIL-4 and 200 U ml⁻¹ rhTNF-α) for 24 h, and the corresponding NVs were prepared according to the DCNV-rAd-Ag preparation procedure.

The presence of NVs was verified through the morphological examination by cryo-electron microscopy, transmission electron microscopy and size measurement using dynamic light scattering (Zetasizer software 7.13). To detect the presence of major functional membrane proteins on the DCNV-rAd-Ag, a western blot assay was performed. Briefly, membrane proteins were extracted from 0.5 ml (1 mg ml⁻¹ total protein) of DCNV-rAd-Ag by a ProteoExtract Transmembrane Protein Extraction Kit (Merck). Samples were probed with antibodies against GFP/OVA, MHC-I, B7-1, B7-2, ICAM-I or CCR7 (all purchased from Invitrogen). The major functional membrane proteins were visualized with an HRP-antimouse/rabbit immunoglobulin G antibody (Invitrogen) and ECL substrate (Thermo). To determine the content of Ag in the total amount of protein, a GFP/OVA ELISA kit or FLAG ELISA kit (Abcam) was used to directly or indirectly quantify the amount of Ag. Membrane proteins on DCs and NVs were extracted and then identified by liquid chromatography/tandem mass spectroscopy analysis. Raw data files were processed using Proteome Discoverer (PD) version 1.4 (Thermo Scientific).

Preparation and characterization of ASPIRE. A signal sequence was fused in the N-terminus of the anti-PD1 *scFv* gene region, and a HIS-Tag was fused before the *scFv* gene region. To facilitate the analyses of epitope expression, a flexible peptide linker (GGGGS)₃ and a PDGFR transmembrane domain were fused to the C terminus. The gene encoding anti-PD1 ScFv was finally cloned into plasmid vector pcDNA3.1(+) to express membrane-localized anti-PD1 antibodies in DCs (αPD1-DC) (Supplementary Fig. 16). Immature DCs transfected with pcDNA3.1(+)-αPD1 (10⁵ cells μg⁻¹) were cultured in the culture medium with the addition of growth factor combination (that is, 1,000 U ml⁻¹ rmGM-CSF and 1,000 U ml⁻¹ rmIL-4). After 48 h of culture, the cells were infected with the recombinant adenovirus mentioned previously (rAd-GFP/OVA, rAd-MultiAgs, rAd-neo), and cultured in the culture medium with the addition of maturation factor combination (1,000 U ml⁻¹ rmGM-CSF, 1,000 U ml⁻¹ rmIL-4 and 200 U ml⁻¹ rmTNF-α) for another 12 h. The cells were collected and NVs were extracted in a similar procedure to that in Preparation and characterization of DCNV-rAd-Ag.

αPD1-DCNV/αPD1-DCNVᴮ⁷⁻/⁻ were prepared after αPD1-DC/αPD1-DCᴮ⁷⁻/⁻ were induced by maturation factor combination with 12 h of incubation. The cells were collected and NVs were extracted in a similar procedure to that in Preparation and characterization of DCNV-rAd-Ag.

To detect the orientation of the αPD-1 antibody on ASPIRE or αPD1-DCNVs, an immunoprecipitation assay was performed. Briefly, 0.5 ml (1 mg ml⁻¹ total protein) of ASPIRE or αPD1-DCNVs were incubated with beads (Santa Cruz Biotechnology) conjugated to protein A/G for 1 h at room temperature after the addition of 2 μg of anti-His antibody specific for the fusion protein HIS-αPD1. The beads were washed gently thrice with PBS. Sample mixtures were resolved and subjected to 10% SDS–PAGE and analysed by western immunoblot assay.

Antigen self-presentation to activate naive CD8+ T cells. To assess the ability of DCNV-rAd-Ag for antigen self-presentation and to directly activate naive T cells, CD8+ T cells (2 × 10⁵ per well) selected from the spleen of C57BL/6 mice were co-cultured with different doses of DCNV-rAd-GFP/293TNV-rAd-GFP/DCNV-Ad/DCNV formulations (0.5, 5 and 20 μg ml⁻¹ NVs) in RPMI 1640 culture medium. After 7 days of incubation, the cells were transferred to ELISPOT plates (Merck), which were pretreated with 95% ethanol and washed with sterile water and PBS before coating with 15 μg ml⁻¹ anti-IFN-γ or anti-TNF-α (Mabtech) overnight at 4 °C. Unbound antibodies were removed by washing with sterile filtered PBS. After 24 h of incubation, the cells were washed away and the plates were incubated with 1 μg ml⁻¹ biotinylated anti-IFN-γ or anti-TNF-α antibody (Mabtech) for 2 h at room temperature. Thereafter, the plates were washed with PBS and incubated for 90 min at room temperature with streptavidin–alkaline phosphatase (Mabtech) (1/1,000 dilution) followed by washing with PBS. The plates were finally incubated with a BCIP/NBT substrate solution (CALBIOCHEM) at room temperature until spots emerged, which took approximately 1 h. The colour development was stopped by repeated washings with tap water. After drying, the spots were counted with an ELISPOT reader using AID ELISPOT software. To detect the activation of primary human T cells, human PBMCs were isolated from healthy blood donors using Ficoll density gradient centrifugation. CD8-positive T cells were isolated by MACS selection (Miltenyi). CD8+ T cells (2 × 10⁵ per well) were co-cultured with different doses of hDCNV-rAd-GFP/293TNV-rAd-GFP/hDCNV-Ad/hDCNV formulations

prepared in PBMCs isolated from the same volunteer (0.5, 5 and 20 µg ml⁻¹ NVs) in RPMI 1640 culture medium. After 7 days of incubation, the cells were transferred to the ELISPOT plates (Merck), and T-cell activation was detected by ELISPOT assay as mentioned above.

To further verify that DCNV-rAd-Ag directly activates T cells and stimulates T-cell specific proliferation, 10^5 OT-I CD8⁺ T cells per well were co-cultured with different doses of DCNV-rAd-OVA and 293TNV-rAd-OVA formulations (0.5, 5 and 20 µg ml⁻¹ NVs) in RPMI 1640 culture medium. After 24 h of incubation, the media were aspirated and 150 µl of CPRG/lysis buffer was added and incubated for 90 min, measured at 570 nm using a microplate reader. The IL-2 and TNF-α in the culture supernatant were determined by a Mouse IL-2 ELISA kit or a TNF-α ELISA kit (both purchased from Dakewe Biotech).

For the detection of T-cell proliferation dilution, an OT-I CD8⁺ T-cell suspension was stained with a carboxyfluorescein succinimidyl ester solution, and co-cultured with 20 µg ml⁻¹ NVs in RPMI 1640 culture medium for 48 h, followed by flow cytometric analysis.

In vivo imaging of DCNVs. For LN draining studies, C57BL/6 mice were treated with DCNV-rAd-OVA@ICG or 293TNV-rAd-OVA@ICG by s.c. injection at the tail base[24,26]. Under isoflurane anaesthesia, in vivo near-infrared fluorescence imaging was performed using an IVIS Lumina II imaging system at 12 h postinjection. C57BL/6 mice were injected with DCNV-rAd-GFP or DCNV-rAd-GFP. After 12 h, inguinal LNs were harvested, and after a 10% formaldehyde solution fixation, paraffin embedding and freezing section, the GFP fluorescence signal was measured.

In vivo immunization and cancer immunotherapy studies. All the mice used for immunological studies were 6–8-week-old females with a C57Bl/6 background. All the animals were cared for and treated according to the instructions and approval of the Institutional Animal Care and Use Committee of Xiamen University (no. XMULAC20190146), and it was defined that the tumour load of mice must not exceed 1.7 cm (diameter). The tumour volume throughout this study was calculated by the equation: tumour volume = length × width² × 0.5. Animals were euthanized when the tumour masses reached 1.5 cm in diameter or when the animals became moribund with severe weight loss or ulceration. C57BL/6 mice were immunized with different formulations: NVs (60 µg per mouse), recombinant adenovirus (2×10^7 vector particles per mouse) or complete dendritic cell vaccine (2×10^5 cells per mouse) in 100 µl by s.c. injection at the tail base at the indicated time points. In some studies, antigen emulsified in AlumOH served as a positive control. Briefly, antigen protein (2 nmol) in 0.5 ml of PBS was thoroughly emulsified in 0.5 ml of AlumOH until the mixture was homogeneous, and then administered subcutaneously in a 100-µl-injection volume.

For prophylactic tumour challenge studies, vaccinated animals were challenged on day 14 after the final immunization by the s.c. injection of 2×10^5 Hep1-6-OVA cells per mouse on the right flank, and tumour growth was monitored every other day. Livers were excised on day 18, followed by enumeration of the Hep1-6-OVA lung tumour nodules. For the CD4⁺/CD8⁺ cell depletion, 250 µg of GK1.5 antibody or 53-6.7 antibody (BioXcell) were administered to the vaccinated tumour-bearing mice by intraperitoneal injection every 2 weeks. For B7-1/2⁻/⁻ mice, vaccinated gene knockout animals were challenged after the final immunization by Hep1-6-OVA cells.

For the therapeutic tumour vaccination studies, C57BL/6 mice were inoculated with 1×10^5 B16F10 or MC-38 cells per mouse on the right flank by s.c. injection on day 0 and vaccinated on the indicated days. For the combinatorial therapy groups, the antimouse PD-1 antibody (10.3 µg per mouse; clone, J43 (BioXcell)) was administered intraperitoneally after each vaccination. For the lung metastasis model, the surviving mice after ASPIRE treatment were rechallenged by the intravenous injection of 5×10^4 B16F10-Luc cells per mouse, and a group of untreated mice were inoculated as a control. Under isoflurane anaesthesia, the fluorescence signal of lungs metastasis was measured every day using an IVIS Lumina II imaging system.

For the co-stimulatory study of the anti-PD1 antibody and B7-1/2, C57BL/6 mice were subcutaneously inoculated with 2×10^5 LLC cells and CD4 depletion was maintained for the duration of the experiment by repeated injections of 250 µg of GK1.5 antibody every 7 days. αPD1-DCNVs were administered by s.c. injection at the tail base every 3 days. For the co-stimulatory study in KO mice, B7-1/2⁻/⁻ mice were inoculated with 1×10^5 MC-38 per mouse by s.c. injection on day 0, and MC-38-specific CTLs were intraperitoneally administered after each vaccination on the indicated days.

For the therapeutic tumour vaccination studies, C57BL/6 mice were inoculated with 1×10^5 MC-38 cells per mouse on the right flank by s.c. injection on day 0, and vaccinated on days 10 and 13 with αPD1-DCNV or DCNV-rAd-neo separately in the order indicated, or vaccinated on day 13 with αPD1-DCNV, DCNV-rAd-neo or ASPIRE (60 µg per dose).

For the antitumour study of ASPIRE in heterogeneous tumours, C57BL/6 mice and antigen-presentation-deficient mice were inoculated subcutaneously with 3×10^5 heterogeneous tumour cells (MC-38-OVA cells mixed with MC-38 cells in various proportions) and vaccinated

with the indicated formulations (60 µg of NVs, 2×10^5 DCs or 0.2 nmol OVA) on days 10, 17 and 24. The mature DCs (CD11c⁺CD80⁺MHCII⁺) in tumour-infiltrating DCs were detected on day 20. Intracellular protein staining and flow cytometric analysis were used for the analysis of OVA in heterogeneous tumour cells at the indicated time points.

Phenotypic and functional assessment of T cells. For the analysis of the activation of peripheral blood lymphocytes, at 2 weeks after the final immunization peripheral blood was harvested from the animals in all the treatment groups. The peripheral blood lymphocytes were prepared and incubated in RPMI 1640 media with 1 µM of the SIINFEKL peptides added. After 24 h, the IL-2/TNF-α/IFN-γ production was measured with the ELISA assay system (purchased from Dakewe Biotech) according to the manufacturer's instructions.

Immunized mice were analysed for the percentages of tumour antigen-specific CD8⁺ T cells using the tetramer staining assay with a peptide–MHC tetramer tagged with PE (H-2Kᵇ-restricted SIINFEKL, MBL Beijing Biotech). Briefly, the peripheral blood lymphocytes were resuspended in a mouse CD16/32 antibody (0.025 mg ml⁻¹) solution to block non-specific and FcR-mediated antibody binding. The suspension was incubate for 10 min at room temperature and washed five times with FACS buffer. Then H-2Kᵇ OVA Tetramer-SIINFEKL-PE solution was added to each sample and incubated for 30 min on ice. Anti-CD8-APC was added to each experimental sample and incubated for 20 min on ice. The samples were washed twice with FACS buffer, fixed and the cells resuspended for flow cytometry analysis. To assess the functionality of the primed CD8⁺ T cells, PBMCs were stimulated ex vivo with the peptide pool (1 µM of each antigen peptide, M27, M30 and TRP2) for 6 h, fixed, permeabilized, stained with anti-IFN-γ-eFluor 660/TNF-α-FITC and anti-CD8-APC, and analysed by flow cytometry.

For the analysis of tumour cells or tumour-infiltrating T cells, tumour tissues were excised at the indicated time points, cut into small pieces of 2–4 mm and then placed in a dissociation buffer (1 mg ml⁻¹ collagenase type IV and 0.1 mg ml⁻¹ DNase I in RPMI) for 30 min at 37 °C with gentle shaking. The cell suspension was passed through a 70 µm strainer, washed with FACS buffer and stained with the indicated antibodies or its isotype control, followed by flow cytometric analysis. The intracellular cytokine staining assays on tumour-infiltrating T cells were performed with anti-IFN-γ-eFluor 660 and anti-TNF-α-FITC.

For the analysis of CD8⁺ T cells in the draining LNs, the draining LNs were excised at the indicated time points. Cell suspensions were prepared and stained with anti-CD8-APC, followed by flow cytometric analysis.

Immunized MC-38 mice were analysed for the percentages of tumour-infiltrating antigen-specific CD8⁺ T cells using a tetramer staining assay with the peptide–MHC tetramer tagged with PE (H-2Kb-restricted ASMTNMELM, MBL Beijing Biotech), functional cell subtypes were analysed by staining with FITC-anti- PD-1/eFluor450-anti-CD38/ PerCP-eFluor710-anti-Granzyme B/FITC-anti-CD44/PE-antimouse CD62L for flow cytometry analysis.

Statistical analysis. All the animal studies were performed after randomization. Experiments were not performed in a blinded fashion. Data were analysed by one- or two-way ANOVA, followed by Bonferroni post hoc test for comparison of multiple groups with Prism (v5.0 and v7.0) (GraphPad Software). Data were normally distributed and the variance between groups was similar. P values less than 0.05 were considered statistically significant. All the values were reported as mean ± s.d. with the indicated sample size. No sample in any representative experiment was excluded from the analysis.

Reporting Summary. Further information on research design is available in the Nature Research Reporting Summary linked to this article.

Data availability
The authors declare that data supporting the findings of this study are available within the article and its Supplementary Information. All the relevant data can be provided by the authors upon reasonable request

Author contributions

C.L. and G.L. conceived and designed the experiments. C.L., Xue Liu, X.X., X.P., S.C., L.Z. and X.W. performed the experiments. C.L., Xue Liu, Xuan Liu, Y.Z., E.R., P.L., X.C. and G.L. analysed the data. C.L., Xue Liu, X.C. and G.L. wrote the manuscript. G.L. supervised the entire project. All the authors discussed the results and edited the manuscript.

Competing interests

G.L. and C.L. are inventors on a patent (No. ZL202010070724.9) related to this study. The other authors declare no competing interests.

Additional information

Supplementary information The online version contains supplementary material available at https://doi.org/10.1038/s41565-022-01098-0.

Correspondence and requests for materials should be addressed to Xiaoyuan Chen or Gang Liu.

Peer review information *Nature Nanotechnology* thanks Michele De Palma, Lana Kandalaft and the other, anonymous, reviewer(s) for their contribution to the peer review of this work.

Reprints and permissions information is available at www.nature.com/reprints.

Corresponding author(s):   Gang Liu; Xiaoyuan Chen

Last updated by author(s): Jan 8, 2022

Reporting Summary

Nature Portfolio wishes to improve the reproducibility of the work that we publish. This form provides structure for consistency and transparency in reporting. For further information on Nature Portfolio policies, see our Editorial Policies and the Editorial Policy Checklist.

Statistics

For all statistical analyses, confirm that the following items are present in the figure legend, table legend, main text, or Methods section.

n/a	Confirmed	
☐	☒	The exact sample size (*n*) for each experimental group/condition, given as a discrete number and unit of measurement
☐	☒	A statement on whether measurements were taken from distinct samples or whether the same sample was measured repeatedly
☐	☒	The statistical test(s) used AND whether they are one- or two-sided *Only common tests should be described solely by name; describe more complex techniques in the Methods section.*
☒	☐	A description of all covariates tested
☐	☒	A description of any assumptions or corrections, such as tests of normality and adjustment for multiple comparisons
☐	☒	A full description of the statistical parameters including central tendency (e.g. means) or other basic estimates (e.g. regression coefficient) AND variation (e.g. standard deviation) or associated estimates of uncertainty (e.g. confidence intervals)
☐	☒	For null hypothesis testing, the test statistic (e.g. *F*, *t*, *r*) with confidence intervals, effect sizes, degrees of freedom and *P* value noted *Give P values as exact values whenever suitable.*
☒	☐	For Bayesian analysis, information on the choice of priors and Markov chain Monte Carlo settings
☒	☐	For hierarchical and complex designs, identification of the appropriate level for tests and full reporting of outcomes
☒	☐	Estimates of effect sizes (e.g. Cohen's *d*, Pearson's *r*), indicating how they were calculated

Our web collection on statistics for biologists contains articles on many of the points above.

Software and code

Policy information about availability of computer code

Data collection	Flow Cytometry: CytExpert (version 2.2); Confocal Imaging:OLYMPUS FV31S-SW v2.3.2.169; In-vivo Imaging:Living Image v4.5.18147; DLS: Zetasizer software 7.13, AID ELISPOT software (version 5.0)
Data analysis	Graphpad Prism (version 5.0 & 7.0); Image J2x (version 2.1.4.7); FlowJo (version 10.0); Snapgene (version 2.3.2), Thermo Scientific Proteome Discoverer (PD) (version 1.4), AID ELISPOT software (version 5.0)

For manuscripts utilizing custom algorithms or software that are central to the research but not yet described in published literature, software must be made available to editors and reviewers. We strongly encourage code deposition in a community repository (e.g. GitHub). See the Nature Portfolio guidelines for submitting code & software for further information.

Data

Policy information about availability of data

All manuscripts must include a data availability statement. This statement should provide the following information, where applicable:

- Accession codes, unique identifiers, or web links for publicly available datasets
- A description of any restrictions on data availability
- For clinical datasets or third party data, please ensure that the statement adheres to our policy

The authors declare that data supporting the findings of this study are available within the article and its Supplementary Information files. All relevant data can be provided by the authors upon reasonable request. The raw and analysed datasets generated during the study are too large to be publicly shared, yet they are available for research purposes from the corresponding author on reasonable request.

Field-specific reporting

Please select the one below that is the best fit for your research. If you are not sure, read the appropriate sections before making your selection.

☒ Life sciences ☐ Behavioural & social sciences ☐ Ecological, evolutionary & environmental sciences

For a reference copy of the document with all sections, see nature.com/documents/nr-reporting-summary-flat.pdf

Life sciences study design

All studies must disclose on these points even when the disclosure is negative.

Sample size	Group size were chosen on the basis of previous experiments using the same methods and were found sufficient to reveal statistically significant differences (as determined using Prism software packages) and biologically relevant differences in the samples of interest. For in vitro cell model and analysis: Rui Kuai, Lukasz J. Ochyl, Keith S. Bahjat, et al. Designer vaccine nanodiscs for personalized cancer immunotherapy. Nat Mater. 2017 Apr;16(4):489-496. doi: 10.1038/nmat4822. For vaccine in vivo distribution: Min Luo, Hua Wang, Zhaohui Wang, et al. A STING-activating nanovaccine for cancer immunotherapy. Nat Nanotechnol. 2017 Jul;12(7):648-654. doi: 10.1038/nnano.2017.52. For Live imaging analysis: Jun Xu, Jia Lv, Qi Zhuang, Zongjin Yang, et al. A general strategy towards personalized nanovaccines based on fluoropolymers for post-surgical cancer immunotherapy. Nat Nanotechnol. 2020 Dec;15(12):1043-1052. doi: 10.1038/s41565-020-00781-4. For anti-tumor treatment: Yuanzeng Min, Kyle C. Roche, Shaomin Tian, et al. Antigen-capturing nanoparticles improve the abscopal effect and cancer immunotherapy. Nat Nanotechnol. 2017 Sep;12(9):877-882. doi: 10.1038/nnano.2017.113.
Data exclusions	No data were excluded from the analyses.
Replication	All experiments were repeated at least three times independently and experimental findings were reproducible.
Randomization	Cells or mice were randomly assigned to different groups before treatment.
Blinding	All the investigators were blinded to group assignment in the course of data collection and analysis.

Reporting for specific materials, systems and methods

We require information from authors about some types of materials, experimental systems and methods used in many studies. Here, indicate whether each material, system or method listed is relevant to your study. If you are not sure if a list item applies to your research, read the appropriate section before selecting a response.

Materials & experimental systems

n/a	Involved in the study
☐	☒ Antibodies
☐	☒ Eukaryotic cell lines
☒	☐ Palaeontology and archaeology
☐	☒ Animals and other organisms
☐	☒ Human research participants
☒	☐ Clinical data
☒	☐ Dual use research of concern

Methods

n/a	Involved in the study
☒	☐ ChIP-seq
☐	☒ Flow cytometry
☒	☐ MRI-based neuroimaging

Antibodies

Antibodies used	anti-mouse CD16/32 Antibody, Biolegend, catalog number:101302, clone number: 93, dilution: 1:200; PE-anti-mouse CD11c Antibody, eBioscience, catalog number: 12-0114-82, clone number: N418, dilution: 1:200; APC-anti-mouse CD80 Antibody, eBioscience, catalog number: 17-0801-82, clone number: 16-10A1, dilution: 1:100; FITC-anti-mouse CD86 Antibody, eBioscience, catalog number: MHCD8601, clone number: BU63, dilution: 1:100; PE-Anti-Mouse MHC Class I (H-2Kb) Antibody, eBioscience, catalog number:12-5958-80, clone number: AF6-88.5.5.3, dilution: 1:200; FITC-Anti-Mouse MHC Class II (I-A/I-E) Antibody, eBioscience, catalog number: 11-5321-82, clone number: M5/114.15.2, dilution: 1:200; PE-Anti-Mouse SIINFEKL/H-2Kb (25-D1.16) Antibody, eBioscience, catalog number: 12-5743-81, clone number: 25-D1.16, dilution: 1:400; eFluor 660-anti-mouse IFN-γ Antibody, eBioscience, catalog number: 50-7311-82, clone number: XMG1.2, dilution: 1:100; FITC-anti-mouse TNF-α Antibody, eBioscience, catalog number: 11-7321-82, clone number: MP6-XT22, dilution: 1:100; APC-anti-mouse CD8 Antibody, Abcam, catalog number: ab288234, clone number: 53-6.7, dilution: 1:100; PE-anti-mouse CD3 Antibody, Abcam, catalog number: ab22268, clone number: KT3, dilution: 1:100; FITC-anti-mouse CD4 Antibody, Abcam, catalog number: ab269349, clone number: GK1.5, dilution: 1:200; FITC-anti-mouse PD-1 Antibody, Abcam, catalog number: ab210291, clone number: J43, dilution: 1:100;

PE-anti-mouse PD-L1 Antibody, Invitrogen, catalog number: 12-5982-83, clone number: MIH5,dilution: 1:100;
eFluor 450-anti-mouse CD38 Antibody, Invitrogen, catalog number: 48-0381-82, clone number: 90, dilution: 1:100;
PerCP-eFluor 710-anti-mouse Granzyme B Antibody, Invitrogen, catalog number: 46-8898-82, clone number: NGZB, dilution: 1:200;
FITC-anti-mouse CD44 Antibody, Invitrogen, catalog number: MA5-17878, clone number: IM7.8.1, dilution: 1:100;
PE-anti-mouse CD62L Antibody, Invitrogen, catalog number: 12-0621-82, clone number: MEL-14, dilution: 1:100;
Mouse IgG2a, monoclonal- Isotype control, Abcam, catalog number: 11-9985-82, clone number: C1.18.4, dilution: 1:1000;
anti-FLAG Antibody, Abcam, catalog number: ab205606, clone number: EPR20018-251, dilution: 1:2000;
anti-HIS Antibody, Abcam, catalog number: ab18184, clone number: HIS.H8, dilution: 1:5000;
anti-GFP Antibody, Invitrogen, catalog number: MA5-15256, clone number: GF28R, dilution: 1:2000;
anti-OVA Antibody, Invitrogen, catalog number: PA1-196, Polyclonal, dilution: 1:1000;
anti-H-2Kb Antibody, Invitrogen, catalog number: MA5-16562, clone number: AF6-88.5, dilution: 1:2000;
anti-B7-1 Antibody, Invitrogen, catalog number: PA5-85913, Polyclonal, dilution: 1:2000;
anti-B7-2 Antibody, Invitrogen, catalog number: PA5-88284, Polyclonal, dilution: 1:2000;
anti-ICAM-I Antibody, Invitrogen, catalog number: MA5407, clone number: 1A29, dilution: 1:5000;
anti-CCR7 Antibody, Invitrogen, catalog number: MA1-163, clone number: 4B12, dilution: 1:2000;
Plasma Membrane Marker (Na/K ATPase, pan Cadherin, PMCA1) Antibody Sampler Panel, Abcam, catalog number: ab254025, dilution: 1:1000;
(HRP) goat anti-mouse IgG antibody, Invitrogen, catalog number: 31430, Polyclonal, dilution: 1:500;
(HRP) goat anti-rabbit IgG antibody, Invitrogen, catalog number: A16096, Polyclonal, dilution: 1:500;
InVivoPlus anti-mouse CD4 BioXcell, catalog number: BP0003-1, clone number: GK1.5
InVivoPlus anti-mouse CD8α BioXcell, catalog number: BP0004-1, clone number: 53-6.7;
InVivoPlus anti-mouse PD-1 (CD279) BioXcell, catalog number: BP0033-2, clone number: J43.

Validation

All antibodies were commercially available and were validated by manufacturers, in previous publications, and in this study, and used for the specifies suggested by the manufacturers.
The invivo administered antibodies were InVivoPlus anti-mouse PD-1 (CD279) (BioXcell , catalog number: BP0033-2, has been tested in vivo for blocking mouse PD-1, https://bxcell.com/product/invivoplus-anti-m-pd-1-cd279/), InVivoPlus anti-mouse CD4 (BioXcell ,catalog number: BP0003-1, has been tested in vivo for blocking mouse CD4, https://bxcell.com/product/invivoplus-anti-m-cd4/), and InVivoPlus anti-mouse PD-1 (CD279) (BioXCell, catalog number: BP0004-1, has been tested in vivo for blocking mouse CD8, https://bxcell.com/product/invivoplus-anti-m-pd-1-cd279/). The fluorescence-labelled primary antibodies used for immunostaining were PE-anti-CD11c Antibody (ebioscience, catalog number: 12-0114-82, has been tested for specificity for mouse CD11c in FACS application, https://www.thermofisher.cn/cn/zh/antibody/product/CD11c-Antibody-clone-N418-Monoclonal/12-0114-82), APC-anti-mouse CD80 Antibody (eBioscience, catalog number: 17-0801-82, has been tested for specificity for mouse CD80 in FACS application, https://www.thermofisher.cn/cn/zh/antibody/product/CD80-B7-1-Antibody-clone-16-10A1-Monoclonal/17-0801-82), FITC-anti-mouse CD86 Antibody (eBioscience, catalog number: MHCD8601, has been tested for specificity for human CD86 in FACS application, https://www.thermofisher.cn/cn/zh/antibody/product/CD86-Antibody-clone-BU63-Monoclonal/MHCD8601), PE-Anti-Mouse MHC Class I (H-2Kb) Antibody (eBioscience, catalog number:12-5958-80, has been tested for specificity for mouse H-2Kb in FACS application, https://www.thermofisher.cn/cn/zh/antibody/product/MHC-Class-I-H-2Kb-Antibody-clone-AF6-88-5-5-3-Monoclonal/12-5958-80), PE-Anti-Mouse SIINFEKL/H-2Kb (25-D1.16) Antibody (eBioscience, catalog number: 12-5743-81, has been tested for specificity for mouse SIINFEKL/H-2Kb in FACS application, https://www.thermofisher.cn/cn/zh/antibody/product/OVA257-264-SIINFEKL-peptide-bound-to-H-2Kb-Antibody-clone-eBio25-D1-16-25-D1-16-Monoclonal/12-5743-81), FITC-Anti-Mouse MHC Class II (I-A/I-E) Antibody (eBioscience, catalog number: 11-5321-82, has been tested for specificity for mouse MHC Class II in FACS application, https://www.thermofisher.cn/cn/zh/antibody/product/MHC-Class-II-I-A-I-E-Antibody-clone-M5-114-15-2-Monoclonal/11-5321-82?imageId=89687), eFluor 660-anti-mouse IFN-γ Antibody (eBioscience, catalog number: 50-7311-82, has been tested for specificity for mouse IFN-γ in FACS application, https://www.thermofisher.cn/cn/zh/antibody/product/IFN-gamma-Antibody-clone-XMG1-2-Monoclonal/50-7311-82?imageId=92429), FITC-anti-mouse TNF-α Antibody (eBioscience, catalog number: 11-7321-82, has been tested for specificity for mouse TNF-α in FACS application, https://www.thermofisher.cn/cn/zh/antibody/product/TNF-alpha-Antibody-clone-MP6-XT22-Monoclonal/11-7321-82), APC-anti-mouse CD8 Antibody (Abcam, catalog number: ab288234, has been tested for specificity for mouse CD8 in FACS application, https://www.abcam.cn/apccy7-cd8-alpha-antibody-53-67-ab288234.html), PE-anti-mouse CD3 Antibody (Abcam, catalog number: ab22268, has been tested for specificity for mouse CD3 in FACS application, https://www.abcam.cn/pe-cd3-antibody-kt3-ab22268.html), FITC-anti-mouse CD4 Antibody (Abcam, catalog number: ab269349, has been tested for specificity for mouse CD4 in FACS application, https://www.abcam.cn/fitc-cd4-antibody-gk15-ab269349.html), FITC-anti-mouse PD-1 Antibody (Abcam, catalog number: ab210291, has been tested for specificity for mouse PD-1 in FACS application, https://www.abcam.cn/pe-pd1-antibody-j431-ab210291.html), PE-anti-mouse PD-L1 Antibody (Invitrogen, catalog number: 12-5982-83, has been tested for specificity for mouse PD-1 in FACS application, https://www.thermofisher.cn/cn/zh/antibody/product/CD274-PD-L1-B7-H1-Antibody-clone-MIH5-Monoclonal/12-5982-83), eFluor 450-anti-mouse CD38 Antibody (Invitrogen, catalog number: 48-0381-82, has been tested for specificity for mouse CD38 in FACS application, https://www.thermofisher.cn/cn/zh/antibody/product/CD38-Antibody-clone-90-Monoclonal/48-0381-82?imageId=92139), PerCP-eFluor 710-anti-mouse Granzyme B Antibody (Invitrogen, catalog number: 46-8898-82, has been tested for specificity for mouse Granzyme B in FACS application, https://www.thermofisher.cn/cn/zh/antibody/product/Granzyme-B-Antibody-clone-NGZB-Monoclonal/46-8898-82?imageId=91942), FITC-anti-mouse CD44 Antibody (Invitrogen, catalog number: MA5-17878, has been tested for specificity for mouse CD44 in FACS application, https://www.thermofisher.cn/cn/zh/antibody/product/CD44-Antibody-clone-IM7-8-1-Monoclonal/MA5-17878), PE-anti-mouse CD62L Antibody (Invitrogen, catalog number: 12-0621-82, has been tested for specificity for mouse CD62L in FACS application, https://www.thermofisher.cn/cn/zh/antibody/product/CD62L-L-Selectin-Antibody-clone-MEL-14-Monoclonal/12-0621-82). The primary antibodies used for Western blot were anti-GFP Antibody (Invitrogen, catalog number: MA5-15256, has been tested for specificity for GFP Tag in Western Blot application, https://www.thermofisher.cn/cn/zh/antibody/product/GFP-Antibody-clone-GF28R-Monoclonal/MA5-15256), anti-OVA Antibody (Invitrogen, catalog number: PA1-196, has been tested for specificity for GFP Tag in Western Blot application, https://www.thermofisher.cn/cn/zh/antibody/product/Ovalbumin-Antibody-Polyclonal/PA1-196), anti-H-2Kb Antibody (Invitrogen, catalog number: MA5-16562, has been tested for specificity for mouse H-2Kb in Western Blot application, https://www.thermofisher.cn/cn/zh/antibody/product/H-2Kb-Antibody-clone-AF6-88-5-Monoclonal/MA5-16562), anti-B7-1 Antibody (Invitrogen, catalog number: PA5-85913, has been tested for specificity for mouse B7-1 in Western Blot application, https://www.thermofisher.cn/cn/zh/antibody/product/CD80-B7-1-Antibody-Polyclonal/PA5-85913), anti-B7-2 Antibody (Invitrogen, catalog number: PA5-88284, has been tested for specificity for mouse B7-2 in Western

Blot application, https://www.thermofisher.cn/cn/zh/antibody/product/CD86-Antibody-Polyclonal/PA5-88284), anti-ICAM-I Antibody (Invitrogen, catalog number: MA5407, has been tested for specificity for mouse ICAM-I in Western Blot application, https://www.thermofisher.cn/cn/zh/antibody/product/ICAM-1-Antibody-clone-1A29-Monoclonal/MA5407), anti-CCR7 Antibody (Invitrogen, catalog number: MA1-163, has been tested for specificity for mouse CCR7 in Western Blot application, https://www.thermofisher.cn/cn/zh/antibody/product/CCR7-Antibody-clone-4B12-Monoclonal/MA1-163). The primary antibodies used for immunofluorescence staining were PE-Anti-Mouse SIINFEKL/H-2Kb (25-D1.16) Antibody (eBioscience, catalog number: 12-5743-81, has been tested for specificity for mouse SIINFEKL/H-2Kb in IF/FACS application), anti-FLAG Antibody (Abcam, catalog number: ab205606, has been tested for specificity for FLAG Tag in IF/IP/FACS applications, https://www.abcam.cn/ddddk-tag-binds-to-flag-tag-sequence-antibody-epr20018-251-ab205606.html), anti-HIS Antibody (Abcam, catalog number: ab18184, has been tested for specificity for HIS Tag in IF/IP applications, https://www.abcam.cn/6x-his-tag-antibody-hish8-ab18184.html), anti-CD16/32 Antibody (to Mouse, IP and Block), can be used for blocking of CD16/CD32 interactions with the Fc domain of immunoglobulins, https://www.biolegend.com/en-us/products/purified-anti-mouse-cd16-32-antibody-190.

Eukaryotic cell lines

Policy information about cell lines

Cell line source(s)	293T HEK, DC2.4, Hep1-6-OVA, B16F10, B16F10-Luc, MC-38, MC-38-OVA and LLC cells were acquired from the National Institute of Diagnostics and Vaccine Development in Infectious Diseases (Xiamen University).
Authentication	The cell lines were certified by the manufacturers (surface markers, morphology). Engineered cell line was verified using negative control and maintained with selection medium according to manufacturer's suggestion.
Mycoplasma contamination	Cell lines were all tested negative for mycoplasma contamination.
Commonly misidentified lines (See ICLAC register)	No commonly misidentified cell lines were used.

Animals and other organisms

Policy information about studies involving animals; ARRIVE guidelines recommended for reporting animal research

Laboratory animals	Six- to eight-week-old male and females C57Bl/6 mice were purchased from SLAC (Shanghai, China). Six- to eight-week-old females B7-1/2-deficient mice with C57BL/6 genetic background were generated by Xiamen University Laboratory Animal Center (XMULAC). Six- to eight-week-old females OT-1 mice were provided by the Chinese Academy of Medical Sciences. The mice were maintained under specific pathogen-free conditions in the animal facility at Xiamen University. Temperatures of 68-74°F with 30-70% humidity are maintained. For monitoring tumour growth, mice were euthanized once the tumors had reached 1.5 cm in size.
Wild animals	No wild animals were used.
Field-collected samples	No field-collected samples were used.
Ethics oversight	All animals received humane care in compliance with institutional and national guidelines. All experimental procedures involving animals were approved by Institutional Animal Care and Use Committee of Xiamen University (NO. XMULAC20190146).

Note that full information on the approval of the study protocol must also be provided in the manuscript.

Human research participants

Policy information about studies involving human research participants

Population characteristics	Healthy male or female volunteers aged 25-45.
Recruitment	Human blood samples were isolated from Chinese healthy adult volunteers with informed consent. No age or gender bias.
Ethics oversight	All experiments using human PBMCs were approved by the Medical Ethics Committee of School of Public Health of Xiamen University.

Note that full information on the approval of the study protocol must also be provided in the manuscript.

Flow Cytometry

Plots

Confirm that:

☒ The axis labels state the marker and fluorochrome used (e.g. CD4-FITC).

☒ The axis scales are clearly visible. Include numbers along axes only for bottom left plot of group (a 'group' is an analysis of identical markers).

☒ All plots are contour plots with outliers or pseudocolor plots.

☒ A numerical value for number of cells or percentage (with statistics) is provided.

Methodology

Sample preparation	As described in the Methods section in detail, fresh tissues (lymph nodes or tumors) were excised at the indicated time points, cut into small pieces of 2-4 mm, and then placed in dissociation buffer (1 mg/ml of collagenase type IV and 0.1 mg/ml of DNase I in RPMI) for 30 min at 37 °C with gentle shaking. The cell suspension was passed through a 70-μm strainer, washed with FACS buffer, and stained with indicated antibodies or its isotype control for 30 min at 4 °C, followed by flow cytometric analysis.
Instrument	CytoFLEX flow cytometer (Beckman Coulter)
Software	Data collection: CytExpert version 2.2 Data analysis: FlowJo version 10.0
Cell population abundance	No cell sorting was performed.
Gating strategy	Gating was first based on FSC/SSC and singlet cells were gated for further analysis. The cell populations were then analyzed based on expression of markers. Gating was then based on positive level.

☒ Tick this box to confirm that a figure exemplifying the gating strategy is provided in the Supplementary Information.